Sedimentary architecture and landforms of the Late Saalian (MIS 6) ice sheet margin, offshore The Netherlands

Víctor Cartelle[1], Natasha L.M. Barlow[1], David M. Hodgson[1], Freek S. Busschers[2], Kim M. Cohen[3], Bart M.L. Meijninger[2], Wessel P. van Kesteren[4]

[1]School of Earth and Environment, University of Leeds, UK
[2]TNO, Geological Survey of the Netherlands, Utrecht, The Netherlands
3Faculty of Geosciences, Utrecht University, Utrecht, The Netherlands
[4]Fugro, Nootdorp, The Netherlands

Correspondence to: Víctor Cartelle (v.cartellealvarez@leeds.ac.uk)

Abstract. Reconstructing the growth and decay of palaeo-ice sheets is critical to understanding the relationships between global climate and sea-level change, and to testing numerical ice sheet models. In this study, we integrate recently acquired high-resolution 2D-seismic reflection and borehole datasets from two windfarm sites offshore The Netherlands to investigate the sedimentary, geomorphological and glaciotectonic records left by the Saalian Drenthe substage glaciation, when Scandinavian land ice reached its southernmost extent in the southern North Sea (ca. 160 ka, Marine Isotope Stage 6). A complex assemblage of glaciogenic sediments and glaciotectonic structures are buried in the shallow subsurface. The northern windfarm site revealed a set of NE-SW oriented subglacial meltwater channels filled with till and glaciofluvial sediments and an E-W trending composite ridge with local evidence of intense glaciotectonic deformation that denotes the maximum limit reached by the ice. Based on the identified glacial geomorphology, we refine the mapping of the maximum ice-sheet extent offshore, revealing that the ice margin morphology is more complex than previously envisaged, and displaying a lobate shape. Ice retreat left an unusual paraglacial landscape characterised by the progressive infilling of topographic depressions carved by ice-driven erosion and a diffuse drainage network of outwash channels. The net direction of outwash was to the west and southwest into a nearby glacial basin. We demonstrate the utility of offshore windfarm data as records of process-form relationships preserved in buried landscapes, which can be utilised in refining palaeo-ice sheet margins and informing longer term drivers of change in low relief settings.

1 Introduction

Reconstructing the growth and decay of palaeo-ice sheets is critical to understanding the relationships between global climate and sea-level change, and to testing numerical ice sheet models (Stokes et al., 2015). Varied types of landforms and deposits are created and preserved by subglacial and proglacial processes, and these can be investigated to reconstruct ice-sheet extent and dynamics. Here, we focus on a distal sector of the penultimate glacial cycle ice sheet (late Marine Isotope Stage [MIS] 6) in NW Europe, located in the North Sea sedimentary basin. The glaciation episode directly preceded the Last Interglacial (LIG; ca. 129-116 ka, MIS 5e) during which global temperatures were ~1ºC warmer than pre-industrial values (Otto-Bliesner et al., 2013), and global mean sea level was likely 6 to 9 m above present (Dutton et al., 2015). Together with climatic forcing and associated ice sheet responses over the MIS 6/5 glacial termination, the distribution of global ice sheets during MIS 6 is critical to understanding the nature of the LIG highstand regionally and globally. This is not trivial as much evidence of MIS 6 glaciation and deglaciations was removed or heavily overprinted by glaciations during the Last Glacial. Thus, the uncertainty in knowing the MIS 6 ice-sheet limits and the timing of deglaciation (Batchelor et al., 2019), represent a weakness in glacial isostatic adjustment modelling, which is needed to understand rates and magnitudes of global and regional LIG RSL change (Barlow et al., 2018; Dendy et al., 2017; Rohling et al., 2017).

The MIS 6 North European ice sheet reached a greater southward and eastward extent compared to the Last Glacial Maximum (LGM, MIS 2), where it had terrestrial limits. Its ocean-limited western extent was smaller than, or similar to, that of the LGM (Batchelor et al., 2019; Ehlers and Gibbard, 2004). Over Germany and The Netherlands, the MIS 6 maximum ice advance was more extensive than the LGM and consequently relatively well preserved; and is known as the Saalian Drenthe substage ice limit in the regional stratigraphic schemes. These ice limits have been studied from spatially disparate field evidence onshore over a series of ice sheet subsectors (e.g. Busschers et al., 2008; Gibbard and Clark, 2011; Van den Berg and Beets, 1987). The MIS 6 limit continues offshore in the southern North Sea, where the current geological constraints on the position of the Saalian maximum ice margin is limited to that visible in first-generation geophysical data (Joon et al., 1990; Laban, 1995; Oele, 1971) and re-processed seismic data originally acquired to map reservoir-geological features at much greater depth (Moreau et al., 2012). Focusing on sub sectors of former ice sheets where high-resolution data is available can lead to greater certainty in ice-sheet extent and provide insights into the highly complex ice marginal dynamics.

A wealth of new offshore geophysical data targeting the shallow subsurface (~0 to 100 m below seafloor) has become available following significant investment into wind energy in the North Sea region. The high-resolution and high-density datasets from windfarm site investigations provide a stimulus for new research into new Quaternary submerged landscapes(e.g. Cotterill et al., 2017; Eaton et al., 2020; Emery et al., 2019; Mellett et al., 2020). In the Dutch sector of the North Sea, two new windfarm sites, Hollandse Kust Noord and Zuid, are located within the previously mapped extent of the main Saalian (MIS 6) ice sheet (Fig. 1). We integrate recently acquired ultra-high-resolution 2D seismic reflection, borehole and cone penetration test (CPT) datasets to investigate the sedimentary, geomorphological and glaciotectonic records left by the MIS 6 glaciation offshore. We use these data to revise previous reconstructions based on older or low-resolution datasets, to constrain the maximum extent of the ice sheet in the marine sector, to provide insights into the regional marginal dynamics of the ice sheet and to investigate the complexity of the near-surface geology of the North Sea and its implications for offshore infrastructure development and palaeogeographical reconstructions.

2 Regional setting

The Hollandse Kust Noord [HKN] and Zuid [HKZ] windfarms are positioned near the southwestern rim of the Cenozoic North Sea Basin (Van Balen et al., 2005; Ziegler, 1994). Its present-day structural configuration is the result of Late Jurassic–Early Cretaceous rifting, followed by thermal cooling and subsidence (Glennie and Underhill, 2009; Zanella and Coward, 2003). Up to 3500 m of Cenozoic sediment has accumulated in the central part of the basin (Knox et al., 2010). Increased Quaternary subsidence has allowed a thick sedimentary succession to accumulate (up to 1250 m thick) (Arfai et al., 2018; Lamb et al., 2018). The Quaternary record thins towards the southern edge of the basin, reaching a thickness of 400 to 800 m at the location of the HKN and HKZ windfarms (Cameron et al., 1984; Knox et al., 2010). The Quaternary record primarily consists of stacked fluvial (primarily Eridanos and Rhine) and shallow marine (water depths up to 300 m, Kuhlmann, 2004) sediments with multiple intercalations of glacial sediments.

The North Sea area experienced several major glaciations during the Quaternary, of which the Elsterian (MIS 12 and/or 10), late Saalian (MIS 6) and late Middle Weichselian (MIS 2) were the most extensive (Busschers et al., 2008; Cameron et al., 1992; Caston, 1979; Dove et al., 2017; Ehlers and Gibbard, 2004; Gandy et al., 2020; Graham et al., 2011; Laban and van der

Meer, 2011; Lauer and Weiss, 2018; Lee et al., 2012; Zagwijn, 1973, 1983). In The Netherlands, the late Saalian ice sheet reached furthest south (Fig. 1). A complex assemblage of glaciogenic sediments and glaciotectonic structures (ice-pushed ridges) surrounding tongue-shaped basins have been identified and studied in the northern and central onshore Netherlands (Bakker, 2004; Bakker and Van der Meer, 2003; Beets et al., 2006; Busschers et al., 2008; Van den Berg and Beets, 1987). Offshore, recorded evidence is scarce, and the reconstruction of the late Saalian ice-sheet maximum extent is based on the study of sediments recovered in limited boreholes and landforms imaged by seismic reflection methods (Graham et al., 2011; Joon et al., 1990; Laban, 1995; Laban and van der Meer, 2011). Large tongue-shaped subglacial basins, smaller subglacial meltwater channel features, and in a few exceptional circumstances, glaciotectonic deformation structures are identified in previous generation low-resolution geophysical data (Joon et al., 1990; Laban, 1995; Oele, 1971). West of the Dutch coastline these have been used to define the southwesternmost Saalian ice-sheet limit near 3.5°E/52.5°N (Fig. 1, Joon et al., 1990). The presumed limits then run parallel to the Dutch coastline (roughly N-S orientation) and eventually continue westward to the British sector along curved trajectories north of 53°N (Fig. 1, Gibbard et al., 2009; Graham et al., 2011; Laban and van der Meer, 2011; Lee et al., 2012; Moreau et al., 2012).

3 Study area, materials and methods

3.1 Study area

The study area lies ~20 km west of the coastline of The Netherlands (Fig. 1) and comprises two windfarm sites, Hollandse Kust Noord (HKN) and Hollandse Kust Zuid (HKZ). The combined area of both sites is ~480 km^2, both are located in shallow waters of less than 30 m and the distance between both windfarm sites is 17 km. Joon et al. (1990) suggest that HKN is positioned inside the maximum Saalian ice limit while HKZ is located on or just beyond the limit. In addition, the two windfarm sites are located between two tongue-shaped glacial basins, a smaller one east of the study area (Bergen basin, Fig. 1) and a much larger one west of the study area (P/Q-block basin, Fig. 1).

3.2 Materials

Geophysical surveys of the HKN and HKZ windfarm development areas were carried out by Fugro between 2016 and 2018 on behalf of The Netherlands Enterprise Agency (RVO). The datasets acquired during these surveys are publicly available and

stored by RVO (www.offshorewind.rvo). The data include both geophysical, geotechnical and geological investigations from several phases. The shallow subsurface is imaged using sub-bottom profiler (SBP), single-channel sparker (SCS) and high-resolution multi-channel sparker (MCS). The line spacing is variable for each system and site. In HKN, the grid line spacing is 100 m in the NE-SW orientation and 2000 m in the NW-SE orientation for SBP and SCS, and 500x500 m for MCS. In HKZ, the grid line spacing is 100 m in the NE-SW orientation and 2000 m in the NW-SE orientation for SBP, and 300 m in the NE-SW orientation and 750 m in the NW-SE orientation for SCS and MCS. Application of tidal corrections for the three systems gives depth relative to the lowest astronomical tide (LAT). Both the SCS and MCS seismic reflection data have been depth converted by Fugro. A velocity of 1600 ms^{-1} was used for the SCS to convert from two-way travel time (TWT) to depth in metres (m below LAT), and the MCS was depth-converted using a velocity field derived during seismic processing (Fugro, 2017a, 2016a, 2016b, 2016c, 2016d). The maximum vertical resolution is 0.7-1.8 m for MCS and 0.5 m for SCS, both with a mean horizontal resolution of 2 m (Fugro, 2017a, 2016a, 2016b, 2016c, 2016d).

The geotechnical investigations included a combination of boreholes (BHs), downhole sampling, and/or *in situ* testing through cone penetration tests (CPTs) at targeted depths of 3 to 80 m. Boreholes were drilled using open-hole rotary drilling. Twenty-eight locations were drilled and sampled in HKN, and 35 in HKZ (Fig. 1). CPTs completed in 66 and 137 locations in HKN and HKZ (Fig. 1), respectively. Data from boreholes is limited to the borehole logs, sample descriptions and photographs provided in reports by Fugro (Fugro, 2019, 2017b, 2017c, 2016e, 2016f). These reports also include results from pollen analyses of a selection of boreholes (StrataData, 2019, 2017). Pollen sampling was low resolution, with only a few samples per borehole, and analyses were conducted on samples that ranged from 5 to 60 cm of sediment.

3.3 Methods

The RVO-provided geophysical and geotechnical datasets (excluding interpretation) are used in this study to investigate the landscape left by the late Saalian glaciation. Interpretation of seismic facies and units was conducted in IHS Kingdom software according to the basic principles of seismic stratigraphy (Mitchum, 1977; Mitchum et al., 1977; Mitchum and Vail, 1977). Seismic facies were characterised following Mellett et al. (2013) and Mitchum et al. (1977) and were used to define seismic stratigraphic units. Key horizons were mapped, interpreted and gridded to maps using the flex gridding algorithm in Kingdom. Infill between key horizons was characterised by their seismic facies (Table 1) and architecture, tied to relevant boreholes and

CPT profiles in key locations. The descriptions of the boreholes were cross-checked with photographs and improved where possible to construct detailed measured sections. Where available, the pollen and palynomorph data generated as part of the Fugro investigations (StrataData, 2019, 2017) were integrated into the analysis to cross-verify and support palaeo-environmental interpretations.

4 Results and interpretation

Three seismic stratigraphic units (U1, U2 and U3) were defined by mapping two key surfaces (S1 and S2) based on the integration of geophysical and geotechnical datasets from both windfarm sites. The seismic unit distribution varies spatially, from north to south across the study area (Fig. 2). The correlation of seismic units between both windfarm sites is based on the nature of their bounding surfaces, their sedimentological characteristics and pollen content. We have also examined available legacy datasets between both windfarm sites, but they showed limited resolution or penetration.

The lower seismic unit (U1) is present throughout the study area. We do not distinguish a basal contact to U1 (Fig. 2). In general, U1 is characterised by a weak acoustic response, and its internal structure is distinguished only locally in its upper part, comprising sub-parallel, low frequency, low-to-medium amplitude reflectors that are truncated by disconformity S1. Seismic unit 2 (U2) is only present in the north of the study area, infilling depressions of S1 (Fig. 2). U2 seismic facies are generally transparent, but some low amplitude reflectors are distinguished to the south onlapping and downlapping the underlying U1. The top of U2 is defined by disconformity S2, which truncates underlying units across the study area (Fig. 2). The overlying seismic unit (U3) thickens southward, where it lies directly over U1, and S1 and S2 are coincident. The seismic facies of U3 are highly variable. Both U1 and U3 comprise several stratigraphic units, but remain undifferentiated in this study for simplicity.

Marked spatial differences in both the internal structure of the seismic units and the morphology of their bounding surfaces exist across the study area (Fig. 2). Hence, we present detailed descriptions geographically and consider three sectors: northern sector of HKN, middle sector of HKN, and southern sector of HKN and the HKZ windfarm, integrating both the geophysical (seismic) and geotechnical (sampled boreholes, CPTs) datasets (Fig. 3).

4.1 Northern sector of HKN

4.1.1 Description

In the northern sector of HKN, the basal seismic U1 is generally characterised by a weak acoustic response, displaying transparent and semi-transparent facies (sf1, Table 1). Locally, discontinuous slightly-wavy or sub-parallel reflectors are observed in the upper part of the unit, truncated by S1 (sf2, Table 1). Most boreholes are located where U1 predominantly displays transparent acoustic facies and comprise silty fine-to-medium sand. Rare dark organic clay and peat were recovered at deeper levels (Fig. 4).

Surface 1 (S1) is characterised by deep V-shaped incisions filled by U2 (Fig. 4). The detailed mapping of S1 in the HKN windfarm site shows a set of elongate depressions, generally oriented NE to SW, and up to 68 m deep (m below LAT, Fig. 3). These depressions are highly irregular in shape, of varied dimensions (0.5 to 8 km long and up to 1 km wide) and are characterised by steep walls (5-20°), an undulating thalweg and abrupt terminations. U2 infills the depressions and is characterised by semi-transparent facies and discontinuous sub-parallel reflectors (sf3, Table 1, line A-A', Fig. 3). A set of three high-amplitude discontinuous reflectors are commonly observed at the base of U2 (sf4, Table 1), corresponding in the boreholes to an admixture of clay, silt, sand and gravel (clay-rich diamicton, Fig. 4), and in CPT logs by low cone resistance values due to the high clay content. The overlying infill corresponds to very dense medium-grained sands, sometimes containing thin laminae of silt and clay (Fugro, 2019). Pollen analyses performed in borehole HKN10 (StrataData, 2019) indicate relatively high numbers of fern and moss spores and freshwater algae, while tree pollen is low and dominated by *Pinus*. Towards the top of U2 (10-12 m in HKN10), moderate numbers of other tree types are also reported, mainly *Alnus*, *Betula*, *Corylus* and thermophilous *Quercus* (StrataData, 2019).

Seismic unit U3 corresponds to the depositional package that onlaps U2 and U1. In general, U3 is thin (<5 m) displays a sheet-like geometry, and locally thickens above isolated depressions (e.g. section A-A' in Fig. 4). Seismic facies of U3 are more distinct on SBP data, displaying parallel, high to medium amplitude reflectors (sf5, Table 1). In boreholes, this unit mainly corresponds to heterolithic interbedded sands and silty sands with abundant shells and shell fragments. These deposits are characterised by relatively high numbers of foraminiferal test linings and dinocysts (StrataData, 2019). Where basal depressions are present, sands overlay dark organic, laminated clayey silts (Fig. 4). Laminated silts recovered at the base of

U3 in borehole HKN10 (Fig. 4) are dominated by tree pollen, mainly *Quercus*, *Pinus*, *Alnus*, *Corylus* and *Betula* (StrataData, 2019).

4.1.2 Interpretation

The most prominent features in the northern sector of the study area are the deep NE-to-SW trending depressions that truncate U1 (Figs. 3 and 4). Their abrupt terminations, the rising and falling thalweg, and the lack of connection between the different depressions means they are unlikely to represent a fluvial channel network. Instead, they are consistent with the features of subglacial meltwater channels and tunnel valleys (Clayton et al., 1999; Kehew et al., 2012; Ó Cofaigh, 1996; van der Vegt et al., 2012), which typically form as the result of erosional processes occurring beneath continental ice sheets. The disrupted aspect of reflectors from the underlying seismic unit (U1, sf2), with some inferred faulting and possibly folding, is interpreted as glaciotectonic deformation of the pre-existing deposits. The patchy high-amplitude reflectors found at the base of the subglacial meltwater channel-fills, corresponding to matrix-supported diamicton in the boreholes, are interpreted as glaciogenic deposits, probably subglacial traction till. These deposits are restricted to the northern sector of HKN and are associated with the subglacial meltwater channels and their margins.

The upper part of U2 is characterised by a weak acoustic signal and occasionally sub-parallel reflectors, mainly corresponding to dense fine and medium sands. The freshwater algae content and the dominance of *Pinus* pollen indicate deposition under cool or cold conditions in a terrestrial or freshwater setting, although the presence of thermophilous species, such as *Quercus*, towards the top of U2, indicates a progressive transition towards a warmer climate. Given the seismic architecture, these sediments are likely to be channel infills laid down after deglaciation..

Boreholes through U3 are characterised by an increase in marine indicators (shells, dynocysts, foraminifera) and tree pollen is abundant at the base (e.g. *Quercus*, StrataData, 2019), indicating mild climatic conditions. Overall, U3 aggrades and drapes older deposits and is interpreted as coastal and/or marine sediments deposited during marine transgression.

4.2 Middle sector of HKN

4.2.1 Description

The middle sector of the HKN windfarm shows local intense deformation where the reflectors of U1 are faulted and distorted (Fig. 5). In this area, the top of U1 occurs < 5 m beneath the seafloor. Although the acoustic signal of U1 is weak, some steeply dipping reflectors (4-15°) are distinguished (sf6, Table 1) that show evidence of intense, southwards and south-westwards verging thrusts (Fig. 5). Mapping this zone of contractional deformation reveals an E-W oriented ridge-like feature denoted by linear topographic highs in the contour map of S1 (Fig. 3). Seismic profiles through this area (Fig. 2 and 5) revealed that the thrust ridge is up to 4 km wide, buried beneath the younger U2 and U3 deposits. Borehole HKN56 is sited on top of this ridge (Fig. 5). Sediments from U1 correspond to laminated sandy clays (from 34 to 39.5 m) with interbedded sand and peat overlain by a thick, massive deposit of dense, silty-fine sand (from 4 to 34 m, HKN56, Fig. 5). Clay and peat beds appear laterally extensive as they are intersected by several boreholes between 36 and 42 m below the seafloor in the middle of HKN. These beds are highlighted in CPT profiles by low cone resistance values and a high friction ratio. These clay and peat deposits are found at the base of the thrust blocks (Fig. 5), delimiting a ~35 m thick package of deformed strata (Fig. 5).

The thrust ridge segment is truncated at the northern flank by an E-W trending incision at the base of U2 (Figs. 3 and 5). Here, seismic facies of U2 are of variable amplitude and frequency, generally with onlapping subparallel reflectors (sf7, Table 1). Several phases of incision and infill can be identified (section C-C', Fig. 5). To the south of the ridge, there is a large E-W-trending depression (Figs. 3 and 5). However, the base of this depression is mainly sub-horizontal and its relationship with underlying strata is not clear. This depression is filled by a set of clinoforms with a southwards progradational trend (Fig. 3) that are characterised by medium to high amplitude, oblique-tangential reflectors (sf8, Table 1, Fig. 5). U1 and U2 are overlain by U3, which in borehole HKN56 corresponds to laminated fine to coarse-grained sands containing abundant bivalve shells and shell fragments (Fig. 5).

4.2.2 Interpretation

The prominent ridge of thrusts, faulted and possibly folded strata (Fig. 3), with highly deformed sediments of U1 preserved a few meters beneath the modern seafloor, is consistent with glaciotectonised sediments marking an ice-sheet advance into this

part of HKN. The glaciotectonised segment is up to 4.5 km wide and glaciotectonic disturbance affects deposits down to 30-40 m below the seafloor, where the extensive peat and clay layers likely form a basal detachment surface (décollement).

The primary E-W direction of the depression that truncates the north flank of the glaciotectonised unit contrasts with the dominant NE-SW drainage direction of the subglacial channels identified in the northern sector of the windfarm (Fig. 3). The acoustic character of U2 here is also different, displaying sub-parallel reflectors and a multiphase history of infill (line C-C', Fig. 5). Our preferred interpretation is that these incisions are proglacial meltwater channels formed during a phase of ice retreat (post-glaciotectonic) that were probably filled by glacial outwash sediments as meltwater discharge eroded and reworked the top of the glaciotectonised ridge and surrounding areas. The interpretation of the depression on the southern side of the glaciotectonic ridge is less clear. It could correspond to an incision due to the erosive action of meltwater or to a syncline that was overthrust from the north and later infilled with outwash deposits. The location, morphology, and internal structure of the southward progradational clinoforms accumulated within this depression supports an interpretation as an outwash fan or a fan-delta that prograded into a proglacial lake. Glaciotectonised and glaciofluvial deposits in this area are buried by a drape of coastal and marine sands (U3, Fig. 5), which thickens to the south (Fig. 2), similar to U3 in the northern sector of HKN.

4.3 Southern sector of HKN and the full HKZ windfarm

4.3.1 Description

We group the southern sector of HKN windfarm and the whole of the HKZ windfarm area together because of their similarity in seismo-stratigraphic architecture, which is characterised by the southward thickening of U3 that is directly overlying U1. U2 is absent and S1 and S2 merge into a single unconformity (Fig. 2). U1 in this sector is generally characterised by more acoustically stratified facies, although the acoustic return is still weak. Parallel horizontal reflectors of low amplitude and high frequency (sf9, Table 1) are common in the upper part of the unit, while transparent or semi-transparent facies are dominant at depth (sf1, Fig. 6). Locally in the HKZ windfarm, some discontinuous reflectors of very-high amplitude (sf4) are identified in U1 (Fig. 7). In the boreholes, the lower part of U1 corresponds to laminated fine- to medium-grained sand containing some interbedded peat (boreholes HKN72 and HKN70, Fig. 6, and borehole HKZ4-BH04, Fig. 7), while the upper part of U1 comprises laminated fine- to medium-grained sands with some thin laminae of clay, and interbedded sandy clays and silty

sands. This is reflected in the CPT response, displaying a highly variable (serrated) cone resistance for interbedded facies. Pollen analyses of samples from the lower part of U1 in boreholes HKN70, HKN72 and HKZ4-BH04 (StrataData, 2019, 2017) show a consistent presence of tree pollen, including *Pinus*, *Alnus*, *Quercus*, *Ulmus* and *Tilia*, with low to moderate numbers of non-tree pollen, spores and freshwater algae. Marine content is minimal and may be reworked. In the upper part of U1, *Pinus* dominates pollen assemblages, with low to moderate numbers of other tree pollen, non-tree pollen, herbaceous pollen and fern spores. Marine taxa are abundant, including dynocysts (such as *Spiniferites* spp.) and foraminiferal test linings (StrataData, 2019, 2017).

U3 in this sector is characterised by sub-horizontal discontinuous reflectors, generally of low amplitude and variable frequency, and a sheet-like geometry. A set of 3 to 4 very high amplitude reflectors (sf4) are sometimes observed at the base of U3 (e.g. section F-F' of Fig. 6, and Fig. 7) and occasionally at shallower depths (e.g. section B-B', Fig. 7). Several erosive surfaces truncate reflectors, and channel-like incisions are observed within the unit (Fig. 7). Boreholes in HKN record up to 10 m of laminated fine- to medium-grained sand and silty sand containing some shell fragments (Fig. 6). In HKZ, U3 is thicker (~25 m in borehole HKN4-BH04) and comprises laminated clays with some thin laminae of sand at the base of the unit, passing upward to medium-grained sands containing abundant shell fragments (Fig. 7). The very high-amplitude reflectors recorded in the seismic data (sf4) correlate to peat layers of variable (~0.2-2 m) thickness (e.g. in boreholes HKN70 and HKZ4-BH04, Figs. 6 and 7). Pollen recovered in the clay and peat at the base of U3 (10-12 m in HKN70 and 20-25 m in HKZ4-BH04) are characterised by an increased presence of tree pollen, with high numbers of *Pinus*, *Quercus*, *Alnus* and *Ulmus* (StrataData, 2019, 2017). Fern and moss spores are also frequent and marine taxa, such as dynocysts, are minimal but present. In borehole HKN70, these deposits are overlain by sands dominated by *Pinus* (StrataData, 2019), which pass upwards to modern shelly marine sands (Fig. 6). Cold and warm tree pollen assemblages alternate up borehole HKZ4-BH04 (10-20 m, StrataData, 2017) with some intervals of increased reworking and marine influence (Fig. 7).

4.3.2 Interpretation

In this area, both U1 and U3 are characterised by a sheet-like geometry and bounded by a smooth and slightly erosive surface (S1+S2) without prominent incisions. Deposits of U1 generally display parallel to sub-parallel reflectors. Deposits from the lower part of U1 contain interbedded peat, abundant tree pollen (including *Quercus*) and minimal marine content, indicating

deposition in a terrestrial setting under mild climatic conditions. In the upper part, the interbedded sands and clays and the abundant marine taxa support the interpretation of these deposits as a near-coastal setting, probably deposited under cooler climatic conditions as the pollen assemblages are dominated by *Pinus*.

The internal structure of U3, characterised by sub-horizontal reflectors displaying a generally aggrading pattern, indicates that these sediments were deposited during a phase of increasing accommodation. However, the existence of several internal erosion surfaces (Fig. 7) indicates that these deposits are not the result of a single phase and point to a complex depositional history. The cyclicity of the pollen successions and the complicated internal structure, with several intercalated levels of peat and multiple lower-order disconformities (Fig. 7), indicate that this unit probably records multiple glacial-interglacial cycles of which mainly coastal and shallow marine deposits were preserved.

4.4 Seismo-stratigraphic and lithostratigraphic interpretation

Integration of geophysical and geotechnical datasets offshore of the Dutch coast allows identification of a major unconformable surface (S1) formed by ice sheet-driven erosion. The analysis also points a single glacial episode to have created this glaciogenic unconformity. Connecting to lithostratigraphic and chronostratigraphic frameworks established for the adjacent onshore (Fig. 1), we equate the disconformity S1 to the Drenthe glaciation episode of the Saalian glacial stage (ca. 160 ka; mid MIS 6), in line with earlier ice-limit studies covering the southern North Sea (Fig. 1, Gibbard et al., 2009; Graham et al., 2011; Joon et al., 1990; Laban and van der Meer, 2011; Moreau et al., 2012).

U1, which is irregularly truncated by S1, spans deposition up to the MIS 6 glaciation. The seismic facies of U1, which is mostly transparent and semi-transparent in nature, but displays low-amplitude sub-parallel reflectors towards the top, indicates it to represent several lithostratigraphic formations. The upper part of U1 is interpreted to correspond to the late Middle Pleistocene (MIS 7 or older) marine Egmond Ground Fm. (Cameron et al., 1992, 1984; Oele, 1971; Rijsdijk et al., 2005; TNO-GSN, 2021) given the presence of marine taxa (Figs. 6 and 7). The lower part of U1 likely corresponds to the early Middle Pleistocene Yarmouth Roads Fm., which is regionally extensive throughout the southern North Sea (Cameron et al., 1984). The Yarmouth Roads Fm. (corresponding to Formation 4.1.1 in Rijsdijk et al., 2005), includes both marine and fluvial facies that mainly consists of fine or medium-grained non-calcareous sands, with variable clay lamination and local intercalations of

reworked peat (Cameron et al., 1984; Rijsdijk et al., 2005; TNO-GSN, 2021). The weak acoustic character of U1 hinders the clear identification of a bounding surface between both formations.

U2 is confined to subglacial meltwater channels and proglacial and deglacial outwash complexes, directly overlying the late Saalian glaciogenic unconformity (S1, Fig. 4). Such glacial and glaciofluvial sediments are assigned to the Drenthe Fm., which includes all glaciogenic deposits of this glaciation episode (Rijsdijk et al., 2005; TNO-GSN, 2021). Till deposits at the base of U2 correspond to the Gieten Member and the overlying glaciofluvial deposits to the Schaarsbergen Member in this formation (Rijsdijk et al., 2005; TNO-GSN, 2021). Chronostratigraphically, these sediments accumulated in the late Saalian (second half of MIS 6); attributed a numeric age from ca. 155 ka onwards following OSL dating by Busschers et al. (2008). This would be time-equivalent with Drenthe-II and Warthe Substages recognised some 250 km to the northeast of our study area (Elbe estuary and German Bight; e.g. Ehlers and Gibbard, 2004).

U3 comprises a complex internal architecture with several minor-order disconformities. Laminated clays and sands, peat beds, and modern shelly marine sands are included in this unit. Basal pollen assemblages point to a warm interglacial or interstadial, dominated by tree pollen with high numbers of *Quercus* (oak), known to have first re-established in the southern North Sea in the Eemian, which set on considerable time after the Drenthe Substage deglaciation (after 130 ka, within MIS 5e). Fluctuating pollen assemblages indicate that U3 records more than one climatic cycle. We interpret that deposition of U3 started during Termination II (MIS 6/5 transition), from the onset of the Eemian interglacial onwards. U3 appears to have recorded climatic oscillations through the Eemian, the Weichselian and into the Holocene, explaining its complicated internal structure. It is topped by the modern seafloor. Future detailed analysis of this unit, using higher-resolution seismic profiles, may allow the differentiation of lithostratigraphic formations.

5 Discussion

5.1 Glaciotectonic structures and the maximum late Saalian ice-sheet extent

The sedimentological, seismic stratigraphic and geomorphic analyses performed in the study area revealed the preservation of a glacial landscape offshore of the Dutch coast. It is characterised by the presence of subglacial meltwater channels and a glaciotectonic ridge in HKN, that can be classified as a composite ridge or thrust-block (push) moraine (<100 m or relief, Aber

et al., 1989; Aber and Ber, 2007; Van der Wateren, 2002, 1995, 1985), which are usually associated with proglacial or sub-marginal glaciotectonics, forming parallel to the ice margins and marking glacier stillstands or readvances (Aber and Ber, 2007; Benn and Evans, 2010).

Some of the most studied late Saalian composite ridges are found in the onshore glacial record in The Netherlands, at the edges of tongue-shaped glacial basins (Fig. 1), and by comparison are generally large, with a total relief exceeding 200 m. The Veluwe ridge along the west side of the IJssel glacial basin (Fig. 1) comprises an up to ~200 m thick package of unconsolidated deformed strata, displaying stacked thrusts close to the ice-contact that transitions into folded strata in the distal areas (Bakker, 2004; Bakker and Van der Meer, 2003; Van der Wateren, 1995). The structural style of deformation in the Veluwe ridge is different to that found in HKN. The features mapped in HKN are similar in nature to the thinner (60-80 m) onshore Utrecht Ridge in the southwestern margin of the Amersfoort basin (Fig. 1) (Aber et al., 1989; Aber and Ber, 2007). This ridge is composed of imbricated thrust blocks of unconsolidated Pleistocene strata striking parallel to the ridge in a package of deformed sediments. The Utrecht ridge is about 2.5 km wide, displays a plateau top, and is slightly asymmetric in cross profile as the southwestern flank grades into a sandur outwash complex. According to van der Wateren (1995), the style of glaciotectonic deformation of the Utrecht ridge is dominated by thrusting. Although the top plateau has been flattened, this is consequence of denudation and erosion, and not due to the ridge being overridden by the ice sheet. If it had been overridden, an overprint of the structural style by subglacial deformation (compressive and extensional) would be expected (Van der Wateren, 1985). Considering the deformation style and geomorphology, the ridge in HKN likely represents an ice-marginal position denoting the ice-sheet maximum extent, similar to the Utrecht ridge.

Similar features are seen in the wider southern North Sea area. The dimensions, seismic structure and depth of the décollement in HKN are also comparable to the Weichselian thrust-block moraines described in the Dogger Bank area (Cotterill et al., 2017; Emery et al., 2019; Phillips et al., 2018) and the Elsterian composite ridges identified in the Dudgeon windfarm offshore north Norfolk, UK (Mellett et al., 2020). Both cases are examples of well-preserved glaciotectonised packages up to 40-50 m thick (bounded by a basal detachment surface visible in seismic profiles) composed by thrusts and folded unconsolidated sediments. In the Dudgeon windfarm and the eastern sector of Dogger Bank, the glaciotectonised sequences form multiple parallel ridges extending over several kilometres, which are interpreted to be the result of surge-related marginal readvances

during overall ice-sheet retreat (Mellett et al., 2020; Phillips et al., 2018). In the western sector of Dogger Bank, there is a single ridge bounding an area of subglacial meltwater channels and streamlined bedforms (lying to the north of the ridge), interpreted as a terminal thrust-block moraine denoting the maximum extent of the British-Irish ice sheet during the Weichselian (Emery et al., 2019).

Large thrust-block moraines are usually found at the margins of surging glacial landsystems formed due to rapid ice advance into proglacial and pre-existent sediments (Evans and Rea, 2005,1999). Surge-type behaviour has gained relevance in the discussion of marginal dynamics of former ice sheets (e.g., Bateman et al., 2015; Boston et al., 2010; Evans et al., 2019, 2020; Graham et al., 2009; Mellett et al., 2020; Phillips et al., 2018; Vaughan-Hirsch and Phillips, 2017). In HKN, a single thrust-block moraine is preserved and likely formed during a surge event when rapid advance of the ice sheet led to the pressurisation of groundwater within the underlying Quaternary sediments. In the northern sector, large subglacial meltwater channels (Figs. 3 and 4) were eroded in response to the over-pressurisation, while in the middle sector, the thick and laterally extensive mud and peat layers facilitated the development of a décollement and thrust staking in front of the advancing ice mass (Figs. 3 and 5). Although glaciotectonic thrust moraines cannot be taken as solely diagnostic of surging activity (Evans and Rea, 2005,1999), the glacial landforms identified in HKN (Fig. 3) is compatible with surging activity and therefore potentially indicative of a scenario of ice-marginal instability triggered by internal ice sheet dynamics rather than by external climatic forcing.

It is reasonable to conclude that the shallow occurrence of U1 in the HKN windfarm occurred in response to thrusting in front of an advancing ice sheet. Given the absence of a clear palaeo ice-sheet signature in sediments preserved further to the south, this glaciotectonised land system likely records the maximum southernmost position of the late Saalian ice sheet (Fig. 8). This contrasts with the location of the MIS 6 ice-sheet limit which has previously been mapped ~50 km south, through the central part of the HKZ (Fig. 8, Joon et al., 1990; Laban, 1995; Laban and van der Meer, 2011), based on indirect evidence observed in legacy seismic profiles. These mainly comprised south and west-dipping reflectors imaged a few meters beneath present-day seafloor (Joon et al., 1990; Laban, 1995), which were inferred to represent ice-pushed ridges, in continuation to those present on land (Fig. 1). This interpretation is not supported by the newly acquired geophysical and geotechnical datasets, which provide higher resolution imaging of the shallow subsurface and show no unequivocal evidence of glaciotectonic

deformation in the HKZ windfarm area (Figs. 2 and 7). Fugro (2017c) also reported a structure in the HKZ windfarm site that could potentially represent glaciotectonic deformation, comprising a thin package of wavy north dipping reflectors. Upon careful examination of the data, this feature is only visible in a single SCS profile, lacks a minimum lateral continuity (as it is not present in any of the parallel profiles to the west or the east) and is associated to channel incisions and infills. Therefore, we cannot confidently attribute this structure to glaciotectonic deformation, as it is not different from any other channel and bars fills which are locally extensive as part of U1 in HKZ. These channel and bar deposits are probably the same structures suggested by Joon et al. (1990) and Laban (1995) to represent ice-pushed ridges.

Our new mapping (Fig. 8) shows the ice margin in the offshore sector to be more irregular than previously presumed, displaying a lobate shape similar to the marginal features mapped onshore (Fig. 1). The lobate shape onshore is explained by the influence of subsurface structural and hydrological conditions, which developed due to contrasting hydraulic conductivities close to the surface (Van den Berg and Beets, 1987; Van der Wateren, 1995, 1985). The onshore glaciotectonic ridges formed in areas covered by coarse-grained fluvial material, where a fine-grained layer in the lower substratum could act as a basal detachment surface, while ice flow was channelised through the glacial basins. The distribution of the glacial basins is controlled primarily by deeper Cenozoic tectonic structures (De Gans et al., 1987; Van der Wateren, 2003). By comparison, no drastic changes in the subglacial bed conditions are expected offshore, as the underlying Cenozoic stratigraphy in the area is dominated by the sandy deposits of the Yarmouth Roads Fm. (Cameron et al., 1984; Laban, 1995). The offshore lobate margin shown in Figure 8B is in part determined by the proposed Saalian margin at the southwestern edge of the comparatively large P/Q-block glacial basin (west of our study area), which was mapped using legacy seismic data (Joon et al., 1990; Laban, 1995).

We highlight an interesting difference between the glaciotectonic ridges surrounding the glacial basins offshore versus onshore. The glaciotectonic ridges in HKN windfarm are oriented perpendicular to the P/Q-block basin, whereas onshore in the central Netherlands, there are large ridges that formed parallel to the basin rims. The latter probably correspond to paraxial ridges which are part of the evolution of hill-hole pairs (Evans et al., 2021). The glaciotectonic ridge identified in HKN seems to continue beyond the limits of the windfarm, and geomorphological features similar to the paraxial ridges may also be present beyond the areas covered by the dataset. It is of interest to investigate this and test if the P/Q-block basin offshore and the equally sized Amersfoort and IJssel basins onshore are indeed of similar glaciotectonic genesis. The current windfarm data

coverage does not allow us to re-evaluate the Saalian margin position through the P/Q-block basin, but given that new-high resolution geophysical data had led to re-evaluation of the margin position through HKN and HKZ, a similar analysis may be considered to assess the presence of a lobate margin, and thereby enhance understanding of ice sheet processes.

5.2 The late Saalian glacial and deglacial phases in the southern North Sea

During the Drenthe Substage, Scandinavian ice advanced from Swedish and Baltic sea source areas into northern Germany and The Netherlands from the ~NE (Ehlers and Gibbard, 2004; Van den Berg and Beets, 1987; Zagwijn, 1973). In The Netherlands, the ice advance during MIS 6 forced the Rhine-Meuse fluvial system to a southerly (proglacial) position where it connected with glacio-fluvial (sandur) systems in front of the ice sheet (Busschers et al., 2008). The ice sheet eventually advanced into nowadays offshore regions of the Dutch coast where it triggered significant erosion, recorded in the HKN windfarm by surface S1 (Figs. 8 and 9A). Over-pressurised subglacial meltwater carved deep V-shaped NE-SW orientated channels beneath the ice sheet, which are well-preserved in the northern sector of HKN (Figs. 3 and 4), and indicate regional ice advance from the northeast (Huuse and Lykke-Andersen, 2000; Moreau et al., 2012; van der Vegt et al., 2012). Several authors suggested that such V-shaped subglacial channels are eroded mainly by pressurised subglacial meltwater rather than direct glacial abrasion (Jørgensen and Sandersen, 2006; van der Vegt et al., 2012). Large-scale glaciotectonic deformation occurred as the ice sheet pushed into, and overrode, pre-existing sediments, leading to the stacking of detached, thrust-bound sediment packages (slices, U1) in the middle sector of HKN (Figs. 5 and 8). The southern flank of the glaciotectonic ridge is covered by a proglacial fan of outwash deposits that prograded into the nearby water-filled depression (Figs. 5 and 9A).

Three phases of Saalian Drenthe ice advance have been postulated. An earliest ice advance from the NE invaded the northern Netherlands and reached a stationary ice margin (Rappol et al., 1989), forming marginal and fluted moraines onshore (Passchier et al., 2010; Van den Berg and Beets, 1987). A further advance then formed the maximum extent limit across the central Netherlands, creating the offshore HKN ridge, the tongues carving the Haarlem and Amsterdam basins and the further tongues pushing up the Utrecht and Veluwe ridges (Figs. 1 and 9A). Besides the geographical position, the dominant NE-SW direction of the subglacial meltwater channels preserved in HKN also indicates that the ice sheet reached the study area in this main phase of ice advance during MIS 6. To the east of the study area, a final phase of readvance followed the main advance, based on large scale NNW-to-SSE fluted till morphology observed in the northeast of The Netherlands ("Hondsrug" ice flow

system; Van den Berg and Beets, 1987) and this appears to have exacerbated ice-marginal meltwater routing along the main advance ice margin (Meinsen et al., 2011). An explanation for this reorganisation in ice flow direction is a proposed change in coalescence of Scandinavian and British ice in the central North Sea (Ehlers, 1990; Kluiving et al., 1991; Rappol et al., 1989). In the HKN windfarm area, there is no direct evidence for a change in ice-flow direction. The glaciotectonic landform preserved in HKN points to a land-based ice sheet that overrode an exposed North Sea basin floor in a terrestrial setting where outwash deposition dominated. We find no indication in HKN or HKZ of clear water lain deposition, that could mark deposition in a hypothesised proglacial lake at the time of maximum extent (Busschers et al., 2008; Hijma et al., 2012).

Following ice retreat from HKN, subglacial channels were exposed, trapping fine-grained outwash sediments in bodies of standing water (U2; Fig. 9B). Overspill channels likely connected the different pools and lakes, explaining the channel-like incisions that are sometimes observed as concave-up reflectors in the upper part of U2 (Fig. 4). In the middle sector of HKN (Fig. 3), outwash channels eroded the northern flank of the glaciotectonic ridge and, locally, its upper boundary (Fig. 5). The presence of outwash deposits seems to be restricted to the north and middle sectors of HKN (Fig. 2). Only a diffuse drainage network can be inferred from mapping surface S1 (Fig. 3), and a few channelised deposits are identified, mainly oriented E-to-W, near the ice-pushed ridge. These outwash channels may have drained west into the large P/Q-block glacial basin (Joon et al., 1990; Laban, 1995; Oele, 1971), which, with its base at 66 m below sea level, likely acted as an effective sink for meltwater and outwash sediments (Fig. 9B). By comparison, in the southern part of HKN and all HKZ, disconformities S1 and S2 are coincident. It is possible that any outwash deposits here were removed/reworked in the late Saalian/early Eemian; Saalian glaciofluvial sediments that incorporated into the Eem Fm. have been reported in the southern North Sea (Laban, 1995). Any glaciofluvial outwash sediments preserved to the south may also be very thin, patchy, and difficult to identify in seismic data.

Passchier et al. (2010) proposed a model of rapid ice retreat because of ice streaming in developing phases of deglaciation (i.e. from ca. 155 ka onwards in the southern North Sea) based upon the presence of meltwater channels incised into the floors of glacial troughs in the southern North Sea. The Hondsrug phase evidence mentioned above could alternatively be explained in this way too. Ice retreat left an unusual landscape preserved in HKN, characterised by the progressive filling of ice-advance and glacio-fluvial drainage depressions with laminated deposits recording postglacial climatic change through the preserved

pollen (Figs. 3 and 4). The landscape is also characterised by a diffuse drainage network where only a few small deglacial channels are identified (Figs. 3 and 5). We interpret that this proglacial landsystem developed due to the presence of dead ice in HKN during deglaciation. Large masses of dead ice likely hindered development of a clear drainage network and favoured the formation of pools and small deglacial lakes that were progressively filled by fine outwash sediments as the ice melted. This interpretation is also coherent with a surge-type glacial behaviour, as distal parts become stagnant after a surge event leaving large masses of dead ice to melt in the formerly glaciated area. However, to improve understanding of ice margin retreat style in this southwest sector of the ice sheet, additional geomorphological and chronological data is needed, particularly towards the west and north of HKN and HKZ.

5.3 The post Saalian landscape

The Saalian glaciation episode in the southern North Sea created a topography that influenced subsequent landscape evolution (Fig. 9C). Onshore, the Last Interglacial (Eemian) Rhine River invaded the IJssel glacial basin and advanced further to the north as the ice sheet retreated, finally draining into the modern North Sea approximately northwest of HKN (Fig. 9C, Busschers et al., 2008, 2007; Peeters et al., 2016). Some of the tongue-shaped basins onshore formed isolated depressions that turned into large lakes, and subsequently brackish lagoons as the sea progressively inundated the terrestrial landscape (Beets and Beets, 2003; Beets et al., 2006; van Leeuwen et al., 2000). The influence of the antecedent topography is observed in our study area by the spatial distribution of U3, reflecting the depth and relief of S1 and the glacial-fluvial deposits (U2). U3 is thicker to the south, where S1+S2 are deeper, displaying a complex internal structure and high variability of facies. However, it thins northward where glaciofluvial deposits and glaciotectonic ridges are preserved at shallow depths beneath the seafloor (Fig. 2). The influence of the antecedent topography is also reflected at a finer scale; for example, U3 in the northern sector of HKN is thicker where it directly overlies the deeper sections of the subglacial meltwater channels (Fig. 4). Future studies of the Eemian and younger sediments (which in this paper are grouped into U3 for simplicity) must consider the underlying Saalian landscape.

5.4 Implications of using windfarm data for palaeogeographic reconstructions

The high-density grid of seismic reflection data available from these new offshore windfarms permits detailed 3D mapping and investigation of preserved palaeo-landscapes. Careful evaluation of new datasets collected in HKN and HKZ reveals a buried glacial landscape that allows us to identify the limit of the maximum Saalian ice advance in this region ~50 km north of where it was previously inferred (Fig. 8B). Large ice-pushed ridges were systematically included in previous palaeogeographic reconstructions, but the new data reveals the absence of evidence to support such interpretation, highlighting the need to revise palaeogeographic reconstructions using legacy seismic reflection data. Similarly, we have identified transparent and semi-transparent seismic facies, which are usually interpreted as subglacial diamicton on formerly glaciated continental margins (Stewart and Stoker, 1990), which correspond to diverse sets of laminated and interbedded glaciofluvial or coastal sedimentary facies (sf1 and sf3, Table 1). These results further highlight the importance of being able to ground truth seismic interpretations. As new high-quality data from windfarms in the North Sea is released and evaluated, large areas are being reinterpreted, which greatly improves our understanding of their geological evolution (e.g. Cotterill et al., 2017; Eaton et al., 2020; Emery et al., 2019; Mellett et al., 2020). The complexity of the near-surface geology of the North Sea is becoming evident. Major changes in the sediment properties occur at meter scale and caution should be taken when using legacy seismic reflection data to evaluate potential offshore windfarm sites.

Our new reconstruction of the main Saalian (MIS 6) glaciation ice limit places it closer to the inferred Elsterian (MIS 12 and/or 10) ice-sheet limit in this sector of the southeastern North Sea Basin (Fig. 1). The new high-resolution data acquired to support windfarm development also shows a new level of detail on the seismic and lithological characteristics of the near-surface geology, which permits better characterisation of Quaternary glacial and interglacial sediments, allowing us to distinguish between the Elsterian and Saalian glaciations. This detail will allow development of a more robust stratigraphic framework, enabling basin-wide correlation with areas that have a strong chronological control. High-resolution offshore windfarm data has permitted us to better understand the distribution of the late Saalian glaciogenic and glaciofluvial deposits, which is critical to understanding the transgression of the North Sea Basin during the late Saalian/early Eemian, the influence on the distribution of depositional environments, and the preservation potential of palaeogeographical and palaeoclimatological archives.

6 Conclusions

Using a dense grid of high-resolution seismic reflection data acquired to support the development of offshore windfarms, we present sedimentological, seismic stratigraphic and geomorphic analyses of a preserved glacial landscape buried in Quaternary sediments, offshore The Netherlands. The data record a major glaciogenic unconformity generated by ice sheet-driven erosion during the later Drenthe glaciation of the Saalian glacial stage (mid MIS 6). Ice-sheet advance and retreat eroded and deformed the underlying strata, which resulted in a complex ice-marginal landform assemblage. A set of NE-SW oriented subglacial channels indicate that the ice likely advanced into the study area from the NE during the main advance of Saalian land ice in this region. Till deposits are widespread in and around the subglacial channels. We interpret the large E-W composite ridge of glaciotectonised strata observed in the middle sector of the study area as a terminal moraine based on its structural style and preservation and the lack of evidence for ice advance any further south, refining the ice limit ~50 km north of its previously mapped position.

Our mapping identifies a lobate shape to the ice margin, which is a consequence of contrasting subglacial bed conditions. We suggest that the preserved landscape assemblage is indicative of a surging ice-sheet terminus. The thrust-block moraine preserved in the study area likely formed during a surge event when rapid advance led to the pressurisation of groundwater within the underlying Quaternary sediments. The surge induced erosion of large subglacial meltwater channels as well as thrust stacking in front of the advancing ice mass. Such sectorial surge-type behaviour along the margin of the European ice sheet at its greatest extent indicates intrinsic ice margin instability, independent of particular external climate forcing. Following ice retreat, subglacial channels were exposed and turned into pools and small lakes, trapping fine-grained outwash sediments (Schaarsbergen Member of the Drenthe Fm.), with a diffuse drainage network of outwash channels identified from seismic mapping. The net direction of outwash is to the west or the southwest, towards a glacial basin to the west. The improved reconstruction of the ice limit in nowadays offshore parts of the North Sea is a valuable addition to the reconstruction of the European ice sheet during MIS 6.

Data availability

Geophysical surveys of the HKN and HKZ windfarm development areas were carried out by Fugro between 2016 and 2018 on behalf of The Netherlands Enterprise Agency (RVO). The datasets generated during these surveys are publicly available and stored by RVO (www.offshorewind.rvo). These datasets are licensed under Creative Commons 4.0 CC-BY-SA.

Author contribution

VC undertook the research and wrote the article. NLMB, DMH, FSB, KMC, BLMM and WPK provided input on the article and supported the original research.

Competing interests

The authors declare that they have no conflict of interest.

Funding

This project has received funding from the European Research Council (ERC) under the European Union's Horizon 2020 research and innovation programme (grant agreement No 802281).

Acknowledgements

This paper forms a contribution to the ERC-funded RISeR project. We thank The Netherlands Enterprise Agency (RVO) for providing the data used in this study free of charge, licensed under Creative Commons 4.0 CC-BY-SA. We also like to thank Marcel Bakker (TNO) and Keith Richards (KrA Stratigraphic) for fruitful discussions regarding the seismic and pollen data. The authors acknowledge PALSEA, a working group of the International Union for Quaternary Sciences (INQUA) and Past Global Changes (PAGES), which in turn received support from the Swiss Academy of Sciences and the Chinese Academy of Sciences.

References

Aber, J. S. and Ber, A.: Chapter 5 Composite ridges, in: Glaciotectonism, Developments in Quaternary Sciences, Volume 6, edited by Aber, J.S. and Ber, A., Elsevier Ltd, 59–82, doi:10.1016/S1571-0866(07)80073-X, 2007.

Aber, J. S., Croot, D. G., and Fenton, M. M.: Glaciotectonic Landforms and Structures, Springer, Dordrecht, Netherlands, doi:10.1007/978-94-015-6841-8, 1989.

Arfai, J., Franke, D., Lutz, R., Reinhardt, L., Kley, J., and Gaedicke, C.: Rapid Quaternary subsidence in the northwestern German North Sea, Sci. Rep., 8, 11524, doi:10.1038/s41598-018-29638-6, 2018.

Bakker, M. A. J.: The internal structure of Pleistocene push moraines. A multidisciplinary approach with emphasis on ground-penetrating radar., Queen Mary, University of London, 180 pp., 2004.

Bakker, M. A. J. and Van der Meer, J. J. M.: Structure of a Pleistocene push moraine revealed by GPR: The eastern Veluwe Ridge, the Netherlands, Geol. Soc. Spec. Publ., 211, 143–151, doi:10.1144/GSL.SP.2001.211.01.12, 2003.

Van Balen, R. T., Houtgast, R. F., and Cloetingh, S. A. P. L.: Neotectonics of the Netherlands: A review, Quat. Sci. Rev., 24, 439–454, doi:10.1016/j.quascirev.2004.01.011, 2005.

Barlow, N. L. M., McClymont, E. L., Whitehouse, P. L., Stokes, C. R., Jamieson, S. S. R., Woodroffe, S. A., Bentley, M. J., Callard, S. L., Cofaigh, C., Evans, D. J. A., Horrocks, J. R., Lloyd, J. M., Long, A. J., Margold, M., Roberts, D. H., and Sanchez-Montes, M. L.: Lack of evidence for a substantial sea-level fluctuation within the Last Interglacial, doi:10.1038/s41561-018-0195-4, 2018.

Batchelor, C. L., Margold, M., Krapp, M., Murton, D. K., Dalton, A. S., Gibbard, P. L., Stokes, C. R., Murton, J. B., and Manica, A.: The configuration of Northern Hemisphere ice sheets through the Quaternary, Nat. Commun., 10, 3713–3713, doi:10.1038/s41467-019-11601-2, 2019.

Bateman, M. D., Evans, D. J. A., Buckland, P. C., Connell, E. R., Friend, R. J., Hartmann, D., Moxon, H., Fairburn, W. A., Panagiotakopulu, E. and Ashurst, R. A.: Last glacial dynamics of the Vale of York and North Sea lobes of the British and Irish Ice Sheet, Proc. Geol. Assoc., 126(6), 712–730, doi:10.1016/J.PGEOLA.2015.09.005, 2015.

Beets, C. . and Beets, D. J.: A high resolution stable isotope record of the penultimate deglaciation in lake sediments below the city of Amsterdam, The Netherlands, Quat. Sci. Rev., 22, 195–207, doi:10.1016/S0277-3791(02)00089-6, 2003.

Beets, D. J., Beets, C. J., and Cleveringa, P.: Age and climate of the late Saalian and early Eemian in the type-area, Amsterdam basin, The Netherlands, Quat. Sci. Rev., 25, 876–885, doi:10.1016/j.quascirev.2005.10.001, 2006.

Benn, D. and Evans, D. J. A.: Glaciers and Glaciation, 2nd edition, Routledge, London, doi:10.4324/9780203785010, 2010.

Van den Berg, M. W. and Beets, D.: Saalian glacial deposits and morphology in the Netherlands., in: Tills and Glaciotectonics, edited by: Meer, J. J. M. van der, A.A. Balkema, Rotterdam., 235.251, 1987.

Boston, C. M., Evans, D. J. A. and Cofaigh, C. Ó.: Styles of till deposition at the margin of the Last Glacial Maximum North Sea lobe of the British–Irish Ice Sheet: an assessment based on geochemical properties of glacigenic deposits in eastern England, Quat. Sci. Rev., 29(23–24), 3184–3211, doi:10.1016/J.QUASCIREV.2010.05.028, 2010.

Busschers, F. S., Kasse, C., van Balen, R. T., Vandenberghe, J., Cohen, K. M., Weerts, H. J. T., Wallinga, J., Johns, C., Cleveringa, P., and Bunnik, F. P. M.: Late Pleistocene evolution of the Rhine-Meuse system in the southern North Sea basin: imprints of climate change, sea-level oscillation and glacio-isostacy, Quat. Sci. Rev., 26, 3216–3248, doi:10.1016/j.quascirev.2007.07.013, 2007.

Busschers, F. S., Van Balen, R. T., Cohen, K. M., Kasse, C., Weerts, H. J. T., Wallinga, J., and Bunnik, F. P. M.: Response of the Rhine-Meuse fluvial system to Saalian ice-sheet dynamics, Boreas, 37, 377–398, doi:10.1111/j.1502-3885.2008.00025.x, 2008.

Cameron, T. D. J., Laban, C., and Schüttenhelm, R. T. E.: Flemish Bight. Sheet 52oN/02oE. Quaternary Geology, 1:250000 series., 1984.

Cameron, T. D. J., Crosby, A., Balson, P. S., Jeffery, D. H., Lott, G. K., Bulat, J., and Harrison, D. J.: United Kingdom Offshore Regional Report: The Geology of the southern North Sea., London, 170 pp., 1992.

Caston, V. N. D.: The Quaternary Sediments of the North Sea, Elsevier Oceanogr. Ser., 24, 195–196, doi:10.1016/S0422-9894(08)71349-7, 1979.

Clayton, L., Attig, J. W. and Mickelson, D. M.: Tunnel channels formed in Wisconsin during the last glaciation, in Glacial Processes Past and Present, edited by: Mickelson, D.W., Attig, J.W., Geological Society of America, vol. 337, 69-82, 1999.

Cotterill, C. J., Phillips, E., James, L., Forsberg, C. F., Tjelta, T. I., Carter, G., and Dove, D.: The evolution of the Dogger Bank, North Sea: A complex history of terrestrial, glacial and marine environmental change, Quat. Sci. Rev., 171, 136–153, doi:10.1016/j.quascirev.2017.07.006, 2017.

Dendy, S., Austermann, J., Creveling, J. R., and Mitrovica, J. X.: Sensitivity of Last Interglacial sea-level high stands to ice sheet configuration during Marine Isotope Stage 6, Quat. Sci. Rev., 171, 234–244, doi:10.1016/j.quascirev.2017.06.013, 2017.

Dove, D., Evans, D. J. A., Lee, J. R., Roberts, D. H., Tappin, D. R., Mellett, C. L., Long, D. and Callard, S. L.: Phased occupation and retreat of the last British–Irish Ice Sheet in the southern North Sea: geomorphic and seismostratigraphic evidence of a dynamic ice lobe, Quat. Sci. Rev., 163, 114–134, doi:10.1016/J.QUASCIREV.2017.03.006, 2017.

Dutton, A., Carlson, A. E., Long, A. J., Milne, G. A., Clark, P. U., DeConto, R., Horton, B. P., Rahmstorf, S., and Raymo, M. E.: Sea-level rise due to polar ice-sheet mass loss during past warm periods, Science, 349, aaa4019, doi:10.1126/science.aaa4019, 2015.

Eaton, S. J., Hodgson, D. M., Barlow, N. L. M., Mortimer, E. J., and Mellett, C. L.: Palaeogeographic changes in response to glacial-interglacial cycles, as recorded in Middle and Late Pleistocene seismic stratigraphy, southern North Sea - White Rose Research Online, J. Quat. Sci., 35, 760-775, doi: 10.1002/jqs.3230, 2020.

Ehlers, J.: Reconstructing the dynamics of the North-west European Pleistocene ice sheets, Quat. Sci. Rev., 9, 71–83, doi:10.1016/0277-3791(90)90005-U, 1990.

Ehlers, J. and Gibbard, P. L. (Eds.): Quaternary Glaciations - Extent and Chronology. part I: Europe., Elsevier, Amsterdam, 488 pp., 2004.

Emery, A. R., Hodgson, D. M., Barlow, N. L. M., Carrivick, J. L., Cotterill, C. J., and Phillips, E.: Left High and Dry: Deglaciation of Dogger Bank, North Sea, Recorded in Proglacial Lake Evolution, Front. Earth Sci., 7, 1–27, doi:10.3389/feart.2019.00234, 2019.

Evans, D. J. A. and Rea, B. R.: Geomorphology and sedimentology of surging glaciers: a land-systems approach, Ann. Glaciol., 28, 75–82, doi:10.3189/172756499781821823, 1999.

Evans, D. J. A. and Rea, B. R.: Surging glacier landsystem, in Glacial Landsystems, edited by: Evans, D.J.A., Arnold, London, 259-288, 2005.

Evans, D. J. A., Roberts, D. H., Bateman, M. D., Ely, J., Medialdea, A., Burke, M. J., Chiverrell, R. C., Clark, C. D. and Fabel, D.: A chronology for North Sea Lobe advance and recession on the Lincolnshire and Norfolk coasts during MIS 2 and 6, Proc. Geol. Assoc., 130(5), 523–540, doi:10.1016/J.PGEOLA.2018.10.004, 2019.

Evans, D. J. A., Atkinson, N. and Phillips, E.: Glacial geomorphology of the Neutral Hills Uplands, southeast Alberta, Canada: The process-form imprints of dynamic ice streams and surging ice lobes, Geomorphology, 350, 106910, doi:10.1016/J.GEOMORPH.2019.106910, 2020.

Evans, D. J. A., Phillips, E. R. and Atkinson, N.: Glacitectonic rafts and their role in the generation of Quaternary subglacial bedforms and deposits, Quat. Res., 1–35, doi:10.1017/QUA.2021.11, 2021.

Fugro: Geophysical Site Investigation Survey. Hollandse Kust (zuid) Wind Farm Development Zone Wind Farm Site I. Report No. GH176-R1., 2016q.

Fugro: Geophysical Site Investigation Survey. Hollandse Kust (zuid) Wind Farm Development Zone Wind Farm Site II. Report No. GH176-R2., 2016b.

Fugro: Geophysical Site Investigation Survey. Hollandse Kust (zuid) Wind Farm Development Zone Wind Farm Site III. Report No. GH176-R3., 2016c.

Fugro: Geophysical Site Investigation Survey. Hollandse Kust (zuid) Wind Farm Development Zone Wind Farm Site IV. Report No. GH176-R4., 2016d.

Fugro: Geotechnical Report. Investigation Data. Geotechnical Borehole Locations, Wind Farm Site I, Hollandse Kust (zuid) Wind Farm Zone, Dutch Sector, North Sea. Report No. N6196/01. Issue 4., 2016e.

Fugro: Geotechnical Report. Investigation Data. Geotechnical Borehole Locations, Wind Farm Site II, Hollandse Kust (zuid) Wind Farm Zone, Dutch Sector, North Sea. Report No. N6196/03. Issue 4., 2016f.

Fugro: Geophysical Site Investigation Survey. Hollandse Kust (noord) Wind Farm Zone Survey 2017. Report No. GH216-R3., 2017a.

Fugro: Geotechnical Report. Investigation Data. Geotechnical Borehole Locations, Wind Farm Site III, Hollandse Kust (zuid) Wind Farm Zone, Dutch Sector, North Sea. Report No. N6196/05. Issue 4., 2017b.

Fugro: Geotechnical Report. Investigation Data. Geotechnical Borehole Locations, Wind Farm Site IV, Hollandse Kust (zuid) Wind Farm Zone, Dutch Sector, North Sea. Report No. N6196/07. Issue 3., 2017c.

Fugro: Geological Ground Model. Wind farm Site III. Hollandse Kust (zuid) Wind Farm Zone, Dutch Sector, North Sea. Report No. N6196/11. Issue 2., 2017d.

Fugro: Geotechnical Report. Investigation Data. Geotechnical Borehole Locations Hollandse Kust (noord) Wind Farm Zone, Dutch Sector, North Sea. Report No. P903749/02. Issue 6., 2019.

Gandy, N., Gregoire, L. J., Ely, J. C., Cornford, S. L., Clark, C. D., and Hodgson, D. M.: Collapse of the last Eurasian Ice Sheet in the North Sea modulated by combined processes of ice flow, surface melt, and marine ice sheet instabilities, J. Geophys. Res. Earth Surf., 126, e2020JF005755, doi:10.1029/2020JF005755, 2020.

De Gans, W., De Groot, T., and Zwaan, H.: The Amsterdam basin, a case study of a glacial basin in The Netherlands., in: Tills and Glaciotectonics, edited by: van der Meer, J. J. M., Bakelma, Rotterdam, The Netherlands, 205–216, 1987.

Gibbard, P. L. and Clark, C. D.: Pleistocene Glaciation Limits in Great Britain, Dev. Quat. Sci., 15, 75–93,doi:10.1016/B978-0-444-53447-7.00007-6, 2011.

Gibbard, P. L., Pasanen, A. H., West, R. G., Lunkka, J. P., Boreham, S., Cohen, K. M., and Rolfe, C.: Late Middle Pleistocene glaciation in East Anglia, England, Boreas, 38, 504–528, doi:10.1111/j.1502-3885.2009.00087.x, 2009.

Glennie, K. W. and Underhill, J. R.: Origin, Development and Evolution of Structural Styles, in: Petroleum Geology of the North Sea; Basic Concepts and Recent Advances: Fourth Edition, edited by: Glennie, K.W., Blackwell Science Ltd, Oxford, UK, 42–84, doi:10.1002/9781444313413.ch2, 2009.

Graham, A. G. C., Stoker, M. S., Lonergan, L., Bradwell, T., and Stewart, M. A.: The Pleistocene Glaciations of the North Sea Basin, Dev. Quat. Sci., 15, 261–278, doi:10.1016/B978-0-444-53447-7.00021-0, 2011.

Graham, A. G. C., Lonergan, L. and Stoker, M. S.: Seafloor glacial features reveal the extent and decay of the last British Ice Sheet, east of Scotland, J. Quat. Sci., 24(2), 117–138, doi:10.1002/JQS.1218, 2009.

Hijma, M. P., Cohen, K. M., Roebroeks, W., Westerhoff, W. E., and Busschers, F. S.: Pleistocene Rhine-Thames landscapes: geological background for hominin occupation of the southern North Sea region, J. Quat. Sci., 27, 17–39, doi:10.1002/jqs.1549, 2012.

Huuse, M. and Lykke-Andersen, H.: Overdeepened Quaternary valleys in the eastern Danish North Sea: Morphology and origin, Quat. Sci. Rev., 19, 1233–1253, doi:10.1016/S0277-3791(99)00103-1, 2000.

Joon, B., Laban, C., and Meer, J. J. M.: The Saalian glaciation in the North Sea, Geol. en Mijnb., 69, 151–158, 1990.

Jørgensen, F. and Sandersen, P. B. E.: Buried and open tunnel valleys in Denmark—erosion beneath multiple ice sheets, Quat. Sci. Rev., 25(11–12), 1339–1363, doi:10.1016/J.QUASCIREV.2005.11.006, 2006.

Kehew, A. E., Piotrowski, J. A., and Jørgensen, F.: Tunnel valleys: Concepts and controversies - A review, Earth-Science Rev., 113, 33–58, doi:10.1016/j.earscirev.2012.02.002, 2012.

Kluiving, S. J., Rappol, M., and Wateren, D. van der: Till stratigraphy and ice movements in eastern Overijssel, The Netherlands, Boreas, 20, 193–205, doi:10.1111/j.1502-3885.1991.tb00150.x, 1991.

Knox, R. W. O. B., Bosch, J. H. A., Rasmussen, E. S., Heilmann-Clausen, C., Hiss, M., De Lugt, I. R., Kasińksi, J., King, C., Köthe, A., Słodkowska, B., Standke, G., and Vandenberghe, N.: Chapter 12 Cenozoic, in: Petroleum Geologial Atlas of the

Southern Permian basin Area, edited by: Doornenbal, J. C. and Stevenson, A. G., EAGE Publications b.v., Houten, 211–223, 2010.

Kuhlmann, G.: High Resolution Stratigraphy and Paleoenvironmental Changes in the Southern North Sea during the Neogene — an Integrated Study of Late Cenozoic Marine Deposits from the Northern Part of the Dutch Offshore Area, Utrecht University, 205 pp., 2004.

Laban, C.: The Pleistocene glaciations in the Dutch sector of the North Sea. A synthesis of sedimentary and seismic data., University of Amsterdam, 194 pp., 1995.

Laban, C. and van der Meer, J. J. M.: Pleistocene glaciation in The Netherlands, Dev. Quat. Sci., 15, 247–260, doi:10.1016/B978-0-444-53447-7.00020-9, 2011.

Lamb, R. M., Harding, R., Huuse, M., Stewart, M., and Brocklehurst, S. H.: The early quaternary north sea basin, J. Geol. Soc. London., 175, 275–290, doi:10.1144/jgs2017-057, 2018.

Lauer, T. and Weiss, M.: Timing of the Saalian- A nd Elsterian glacial cycles and the implications for Middle-Pleistocene hominin presence in central Europe, Sci. Rep., 8, 1–13, doi:10.1038/s41598-018-23541-w, 2018.

Lee, J. R., Busschers, F. S., and Sejrup, H. P.: Pre-Weichselian Quaternary glaciations of the British Isles, The Netherlands, Norway and adjacent marine areas south of 68°N: Implications for long-term ice sheet development in northern Europe, Quat. Sci. Rev., 44, 213–228, doi:10.1016/j.quascirev.2010.02.027, 2012.

van Leeuwen, R. J. W., Beets, D. J., Bosch, J. H. A., Burger, A. W., Cleveringa, P., van Harten, D., Herngreen, G. F. W., Kruk, R. W., Langereis, C. G., Meijer, T., Pouwer, R., and de Wolf, H.: Stratigraphy and integrated facies analysis of the Saalian and Eemian sediments in the Amsterdam-Terminal borehole, the Netherlands, Netherlands J. Geosci., 79, 161–196, doi:10.1017/S0016774600023647, 2000.

Meinsen, J., Winsemann, J., Weitkamp, A., Landmeyer, N., Lenz, A., and Dölling, M.: Middle Pleistocene (Saalian) lake outburst floods in the Münsterland Embayment (NW Germany): Impacts and magnitudes, Quat. Sci. Rev., 30, 2597–2625, doi:10.1016/j.quascirev.2011.05.014, 2011.

Mellett, C. L., Hodgson, D. M., Plater, A. J., Mauz, B., Selby, I., and Lang, A.: Denudation of the continental shelf between Britain and France at the glacial–interglacial timescale, Geomorphology, 203, 79–96, doi:10.1016/j.geomorph.2013.03.030, 2013.

Mellett, C. L., Phillips, E., Lee, J. R., Cotterill, C. J., Tjelta, T. I., James, L., and Duffy, C.: Elsterian ice-sheet retreat in the southern North Sea: antecedent controls on large-scale glaciotectonics and subglacial bed conditions, Boreas, 49, 129–151, doi:10.1111/bor.12410, 2020.

Mitchum, R. M. J.: Seismic Stratigraphy and Global Changes of Sea Level, Part 11: Glossary of Terms used in Seismic Stratigraphy, in: Seismic Stratigraphy – Applications to Hydrocarbon Exploration, American Association of Petroleum Geologists Memoir 26, edited by: Payton, C. E., American Association of Petroleum Geologists, 135–144, doi: 10.1306/M26490C13, 1977.

Mitchum, R. M. J. and Vail, P. R.: Seismic Stratigraphy and Global Changes of Sea Level, Part 7: Seismic Stratigraphic Interpretation Procedure, in: Seismic Stratigraphy – Applications to Hydrocarbon Exploration, American Association of Petroleum Geologists Memoir 26, edited by: Payton, C. E., American Association of Petroleum Geologists , doi: 10.1306/M26490C9, 135–144, 1977.

Mitchum, R. M. J., Vail, P. R., and Samgree, J. B.: Seismic Stratigraphy and Global Changes of Sea Level, Part 6: Stratigraphic interpretation of seismic reflections patterns in depositional sequences, in: Seismic Stratigraphy – Applications to Hydrocarbon Exploration, American Association of Petroleum Geologists Memoir 26, edited by: Payton, C. E., American Association of Petroleum Geologists, doi: 10.1306/M26490C8, 117–133, 1977.

Moreau, J., Huuse, M., Janszen, A., Vegt, V. Der, Gibbard, P. L., and Moscariello, A.: The glaciogenic unconformity of the southern North Sea, Geol. Soc. Spec. Publ., 368, 99–110, doi:10.1144/SP368.5, 2012.

Ó Cofaigh, C.: Tunnel valley genesis, Prog. Phys. Geogr. Earth Environ., 20(1), 1–19, doi:10.1177/030913339602000101, 1996.

Oele, E.: The Quaternary geology of the southern area of the Dutch part of the North Sea., Geol. en Mijnbouw/Netherlands J. Geosci., 50, 461–474, 1971.

Otto-Bliesner, B. L., Rosenbloom, N., Stone, E. J., Mckay, N. P., Lunt, D. J., Brady, E. C., and Overpeck, J. T.: How warm was the last interglacial? new model-data comparisons, Philos. Trans. R. Soc. A Math. Phys. Eng. Sci., 371, doi:10.1098/rsta.2013.0097, 2013.

Passchier, S., Laban, C., Mesdag, C. S., and Rijsdijk, K. F.: Subglacial bed conditions during Late Pleistocene glaciations and their impact on ice dynamics in the southern North Sea, Boreas, 39, 633–647, doi:10.1111/j.1502-3885.2009.00138.x, 2010.

Peeters, J., Busschers, F. S., and Stouthamer, E.: Fluvial evolution of the Rhine during the last interglacial-glacial cycle in the southern North Sea basin: A review and look forward, Quat. Int., 357, 176–188, doi:10.1016/j.quaint.2014.03.024, 2015.

Peeters, J., Busschers, F. S., Stouthamer, E., Bosch, J. H. A., Van den Berg, M. W., Wallinga, J., Versendaal, A. J., Bunnik, F. P. M., and Middelkoop, H.: Sedimentary architecture and chronostratigraphy of a late Quaternary incised-valley fill: A case study of the late Middle and Late Pleistocene Rhine system in the Netherlands, Quat. Sci. Rev., 131, 211–236, doi:10.1016/j.quascirev.2015.10.015, 2016.

Phillips, E., Cotterill, C., Johnson, K., Crombie, K., James, L., Carr, S., and Ruiter, A.: Large-scale glacitectonic deformation in response to active ice sheet retreat across Dogger Bank (southern central North Sea) during the Last Glacial Maximum, Quat. Sci. Rev., 179, 24–47, doi:10.1016/j.quascirev.2017.11.001, 2018.

Rappol, M., Haldorsen, S., Jørgensen, P. M., Meer, J. van der, and Stoltenberg, H.: Composition and origin of petrographically-stratified thick till in the northern Netherlands and a Saalian glaciation model for the North Sea Basin, Meded. - Werkgr. voor Tert. en Kwartaire Geol., 26, 31–64, 1989.

Rijsdijk, K. F., Passchier, S., Weerts, H. J. T. T., Laban, C., van Leeuwen, R. J. W. W., and Ebbing, J. H. J. J.: Revised Upper Cenozoic stratigraphy of the Dutch sector of the North Sea Basin: towards an integrated lithostratigraphic, seismostratigraphic

and allostratigraphic approach, Netherlands J. Geosci. - Geol. en Mijnb., 84, 129–146, doi:10.1017/S0016774600023015, 2005.

Rohling, E. J., Hibbert, F. D., Williams, F. H., Grant, K. M., Marino, G., Foster, G. L., Hennekam, R., de Lange, G. J., Roberts, A. P., Yu, J., Webster, J. M., and Yokoyama, Y.: Differences between the last two glacial maxima and implications for ice-sheet, δ18O, and sea-level reconstructions, Quet. Sci. Rev., 176, 1-28, doi:10.1016/j.quascirev.2017.09.009, 2017.

Sejrup, H. P., Larsen, E., Haflidason, H., Berstad, I. M., Hjelstuen, B. O., Jonsdottir, H. E., King, E. L., Landvik, J., Longva, O., Nygard, A., Ottesen, D., Raunholm, S., Rise, L., and Stalsberg, K.: Configuration, history and impact of the Norwegian Channel Ice Stream, Boreas, 32, 18–36, doi:10.1080/03009480310001029, 2003.

Stewart, F. S. and Stoker, M. S.: Problems associated with seismic facies analysis of diamicton-dominated, shelf glacigenic sequences, Geo-Marine Lett. 1990 103, 10(3), 151–156, doi:10.1007/BF02085930, 1990.

Stokes, C. R., Tarasov, L., Blomdin, R., Cronin, T. M., Fisher, T. G., Gyllencreutz, R., Hättestrand, C., Heyman, J., Hindmarsh, R. C. A., Hughes, A. L. C., Jakobsson, M., Kirchner, N., Livingstone, S. J., Margold, M., Murton, J. B., Noormets, R., Peltier, W. R., Peteet, D. M., Piper, D. J. W., Preusser, F., Renssen, H., Roberts, D. H., Roche, D. M., Saint-Ange, F., Stroeven, A. P., and Teller, J. T.: On the reconstruction of palaeo-ice sheets: Recent advances and future challenges, Quet. Sci. Rev., 125, 15-49, doi:10.1016/j.quascirev.2015.07.016, 2015.

StrataData: Geochronology of boreholes from Hollandse Kust (zuid) Wind Farm Zone, Dutch Sector, North Sea. Report No: 08/17 (final version), Ottershaw, 2017.

StrataData: Geochronology of boreholes from Hollandse Kust (noord) Wind Farm Zone, Dutch Sector, North Sea. Report No: 10/18 (final version), Ottershaw, 2019.

TNO-GSN: Stratigraphic Nomenclature of the Netherlands, TNO-Geological Survey of the Netherlands: http://www.dinoloket.nl/en/stratigraphic-nomenclature/, last access: 1 June 2021.

Toucanne, S., Zaragosi, S., Bourillet, J. F., Cremer, M., Eynaud, F., Van Vliet-Lanoë, B., Penaud, A., Fontanier, C., Turon, J. L., Cortijo, E., and Gibbard, P. L.: Timing of massive “Fleuve Manche” discharges over the last 350 kyr: insights into the European ice-sheet oscillations and the European drainage network from MIS 10 to 2, Quat. Sci. Rev., 28, 1238–1256, doi:10.1016/j.quascirev.2009.01.006, 2009

Vaughan-Hirsch, D. P. and Phillips, E. R.: Mid-Pleistocene thin-skinned glaciotectonic thrusting of the Aberdeen Ground Formation, Central Graben region, central North Sea, J. Quat. Sci., 32(2), 196–212, doi:10.1002/jqs.2836, 2017.

van der Vegt, P., Janszen, A., and Moscariello, A.: Tunnel valleys: Current knowledge and future perspectives, Geol. Soc. Spec. Publ., 368, 75–97, doi:10.1144/SP368.13, 2012.

Van der Wateren, D. F. M.: A model of glacial tectonics, applied to the ice-pushed ridges in the central Netherlands., Bull. Geol. Soc. Denmark, 34, 55–74, 1985.

Van der Wateren, D. F. M.: Structural geology and sedimentology of push moraines., Meded. Rijks Geol. D., 54, 1995.

Van der Wateren, D. F. M.: Processes of glaciotectonism, in: Modern and Past Glacial Environments, edited by: Menzies, J., Butterworth-Heinemann, Oxford, UK, 417–443, doi:10.1016/b978-075064226-2/50017-9, 2002.

Van der Wateren, D. F. M.: Ice-marginal terrestrial landsystems: southern Scandinavian ice sheet margin., in: Glacial Landsystems, edited by: Evans, D. J. A., Routledge, London, 166–203, 2003.

Zagwijn, W. H.: Pollen-analytical studies of Holsteinian and Saalian beds in the Northern Netherlands., Meded. Rijks Geol. D., 24, 139–156, 1973.

Zagwijn, W. H.: Sea-level changes in the Netherlands during the Eemian., Geol. en Mijnb., 62, 437–450, 1983.

Zagwijn, W. H.: An analysis of Eemian climate in western and central Europe, Quat. Sci. Rev., 15, 451–469, doi:10.1016/0277-3791(96)00011-X, 1996.

Zanella, E. and Coward, M. P.: Structural framework., in: The Millenium Atlas: Petroleum Geology of the Central and Northern North Sea, edited by: Evans, D., Graham, C., Armour, A., and Bathurst, P., The Geological Society of London, London, 45–59, 2003.

Ziegler, P. A.: Cenozoic rift system of Western and Central Europe: an overview, Geol. en Mijnb., 73, 99–127, 1994.

Table 1. Summary of seismic facies identified in the study area.

Seis. facies	Units	Amplitude	Frequency	Continuity	Reflector termination	Structure or fill	Image
sf1	U1	Low	Low	Low	Not applicable	Structureless, transparent to semi-transparent	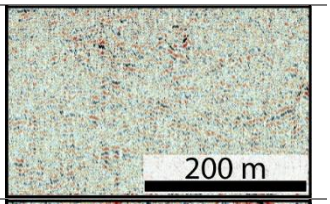
sf2	U1	Low to medium	Low	Low	Truncation	Sub-parallel to wavy	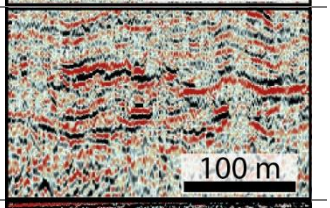
sf3	U2	Low	Low	Low	Onlap and truncation	Semi-transparent with sporadic reflectors	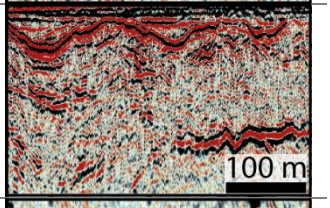
sf4	U1, U2, U3	High	Medium	High	Not applicable	Parallel	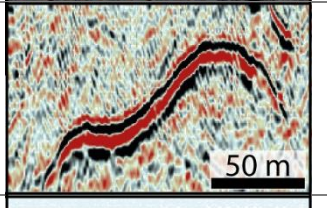
sf5	U3	Medium to high	Medium	High	Base: onlap Top: truncation	Parallel, channelised	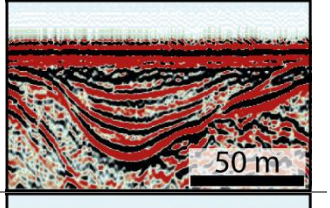
sf6	U1	Low	Low	Low	Top: truncation	Semi-transparent, dipping reflectors, thrusting	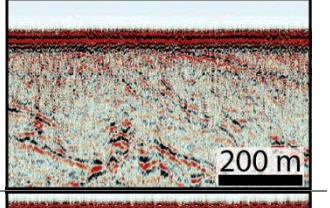
sf7	U2	Medium	Low to medium	Medium to high	Base: onlap, downlap Top: truncation	Channel complex	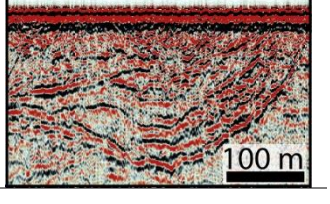

sf8	U2	Medium	Low	High	Base: downlap Top: truncation	Oblique-tangential clinoforms	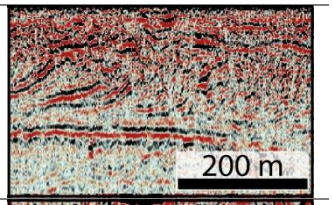
sf9	U1, U3	Low to medium	High	High	Truncation	Parallel, drape	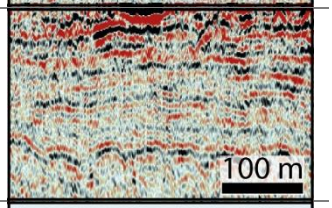
sf10	U3	Low	Variable	Low	Onlap	Sub-parallel, sheet	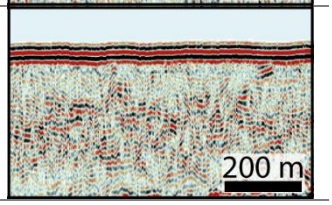

Figure captions

Figure 1. Location of the study area in the southern North Sea showing the Hollandse Kust Noord (HKN) and Zuid (HKZ) windfarm areas. The offshore maximum ice-sheet extension for the Weichselian (Marine Isotope Stage [MIS] 2), late Saalian (MIS 6; Drenthe Substage) and Elsterian (MIS 12 and/or 10) glaciations is displayed (modified from Batchelor et al., 2019; Graham et al., 2011; Hijma et al., 2012; Joon et al., 1990; Laban, 1995; and Moreau et al., 2012). The seismic tracklines displayed correspond to the multi-channel sparker data. Onshore and offshore features compiled from Laban and van der Meer (2011), Joon et al. (1990) and Peeters et al. (2016). Modern bathymetry and topography from GEBCO (https://www.gebco.net).

Figure 2. Representative seismic profiles (multi-channel sparker) and interpretation panels across Hollandse Kust Noord (HKN, above) and Hollandse Kust Zuid (HKZ, below) windfarm areas showing the main seismic stratigraphic units and surfaces. The separation distance between the northern (HKN) and southern (HKZ) profiles is 17 km. For location of the seismic profiles see the inset maps. Depth in meters below Lowest Astronomical Tide (LAT).

Figure 3. Seismic mapping and geological interpretation of HKN windfarm site. Left: Map of the depth of surface S1 (base of unit U2, see also Figs. 2 and 4). Right: Landform interpretation showing subglacial meltwater channels, ice-pushed ridges, till deposits and an outwash fan mapped in the study area. Meltwater direction during the early deglaciation has been inferred from the general relief and slope of surface S1 and the distribution of glaciofluvial deposits.

Figure 4. Stratigraphic section (multi-channel sparker) through subglacial meltwater channels in the northern sector of HKN windfarm area. Borehole HKN10 was recovered in one of these channels capturing the sedimentary characteristics of the three main seismic stratigraphic units. Only the upper 50 m of the borehole are shown. Cone resistance from a CPT obtained in the same site is displayed on the side of the borehole and in the seismic profiles. For location of the seismic profiles and the borehole see the inset map (same map from Fig. 3). Grain size: C – clay, St – silt, fS – fine sand, mS – medium sand, cS – coarse sand, G – gravel. Vertical dashed line indicates the position where the seismic profiles cross each other.

Figure 5. Stratigraphic sections (multi-channel sparker) through the glacio-tectonic ridge in the middle sector of HKN windfarm area. In seismic section C-C', the side of the ridge is incised by proglacial meltwater channel fills. Borehole HKN56 was recovered at the top of the ridge. Only the upper 50 m of the borehole are shown. Cone resistance from a CPT obtained in the same site is displayed on the side of the borehole and in the seismic profiles. In section D-D', outwash sediments (outwash fan) prograde inside a shallow depression incised in the south flank of the ridge. For location of the seismic profiles and the borehole see the inset map (same map from Fig. 3). Grain size: C – clay, St – silt, fS – fine sand, mS – medium sand, cS – coarse sand, G – gravel.

Figure 6. Stratigraphic sections (multi-channel sparker) in the southern sector of HKN windfarm area where unit U3 is directly lying on unit U1 (i.e. surfaces S1 and S2 seismically inseparable). Only the upper 50 m of the boreholes are shown. Cone resistance from CPTs obtained in the same sites is displayed on the side of the boreholes and in the seismic profiles. For location of the seismic profiles and the borehole see the inset map (same map from Fig. 3). The southern limit of unit U2 is also displayed on the map. Grain size: C – clay, St – silt, fS – fine sand, mS – medium sand, cS – coarse sand, G – gravel.

Figure 7. Representative seismic profiles showing the stratigraphy underlying the HKZ windfarm site. Section A-A' corresponds to a multi-channel sparker line, section B-B' to a single-channel sparker line. Borehole HKZ4-BH04 illustrates the sedimentological characteristics of units U1 and U3 in this windfarm. Only the upper 50 m of the borehole are shown. Cone resistance from a CPT obtained in the same site is displayed on the side of the borehole and in the seismic profiles. For location of the seismic profiles and the borehole see the inset map. Grain size: C – clay, St – silt, fS – fine sand, mS – medium sand, cS – coarse sand, G – gravel. Vertical dashed line indicates the position where the seismic profiles cross each other.

Figure 8. (A) Conceptual model of the infill (following transgression from MIS 6 to MIS 5e, but before the highstand) showing the main glacial geomorphological features and sediments preserved in HKN windfarm. (B) Comparison between the previously inferred maximum Saalian ice sheet extent (dashed line, Hijma et al, 2012, Batchelor et al., 2019) and the new limit proposed in this study (solid line). Question marks indicate sectors where the limit is uncertain and more research is needed (see text for details). Channel and bar fills identified in HKZ windfarm are also indicated (some of them formerly interpreted as glaciotectonic ridges). Sources for onshore and offshore features as in Fig. 1. (C) Bathymetry profile through the HKN windfarm area highlighting the glacial geomorphological features identified and the approximate position of the ice front during the maximum ice sheet extent.

Figure 9. Palaeogeographic maps depicting the landscape evolution in the study area. Inset maps show the detailed evolution reconstructed in Hollandse Kust Noord (HKN) windfarm site. (A) Palaeogeography during maximum ice-sheet extent in the Saalian Drenthe substage ca. 160 ka (Busschers et al., 2008; Toucanne et al., 2009). Ice advancing into HKN deformed the underlying strata and carved subglacial meltwater channels. An E-W oriented glaciotectonic ridge indicates the position of the maximum ice front. A contemporary proglacial lake has been proposed in earlier work (Busschers et al., 2008; Hijma et al., 2012), but no evidence/confirmation has been found in this study. (B) Saalian Drenthe substage deglaciation ca. 155 ka (Busschers et al., 2008; Toucanne et al., 2009). Overspilling, interconnected lakes of varied dimensions occupied the deglaciated tongue basins (Beets et al., 2006; Busschers et al., 2008; Laban, 1995; van Leeuwen et al., 2000; Zagwijn, 1996, 1983), as well as smaller-scale subglacial channels. The Rhine river diverted into a larger basin in the east of the depicted area. Drainage in the HKN study area was mainly directed to the larger 'P/Q' tongue basin lake in the west. (C) Latest Saalian to early Eemian North Sea transgression phase, depicted for a sea-level elevation of 30 m below present-day level. Coastal to marine transgressive deposits buried the Saalian glacial landscape in the study area (Peeters et al. 2016, 2015; Van Leeuwen et al. 2000; Zagwijn, 1983). The distribution of these deposits and the timing of the flooding is conditioned by the antecedent topography inherited from the late Saalian glaciation.

Figure 1

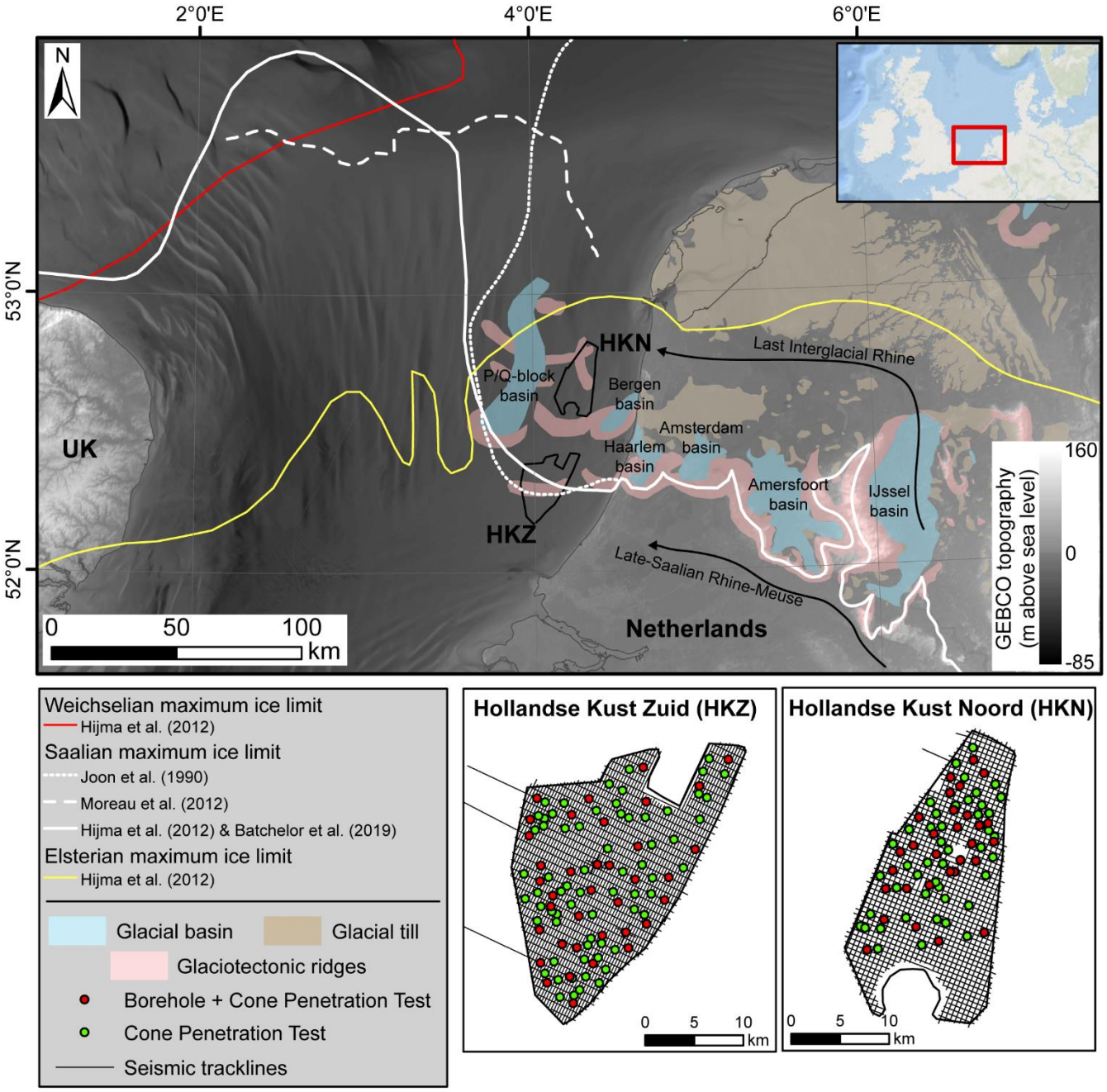
2°0'E
4°0'E
6°0'E
53°0'N
52°0'N
N
UK
HKN
HKZ
P/Q-block basin
Bergen basin
Amsterdam basin
Haarlem basin
Amersfoort basin
IJssel basin
Last Interglacial Rhine
Late-Saalian Rhine-Meuse
Netherlands
0 50 100 km
GEBCO topography (m above sea level)
160
0
-85
Weichselian maximum ice limit
Hijma et al. (2012)
Saalian maximum ice limit
Joon et al. (1990)
Moreau et al. (2012)
Hijma et al. (2012) & Batchelor et al. (2019)
Elsterian maximum ice limit
Hijma et al. (2012)
Glacial basin
Glacial till
Glaciotectonic ridges
Borehole + Cone Penetration Test
Cone Penetration Test
Seismic tracklines
Hollandse Kust Zuid (HKZ)
0 5 10 km
Hollandse Kust Noord (HKN)
0 5 10 km

Figure 2

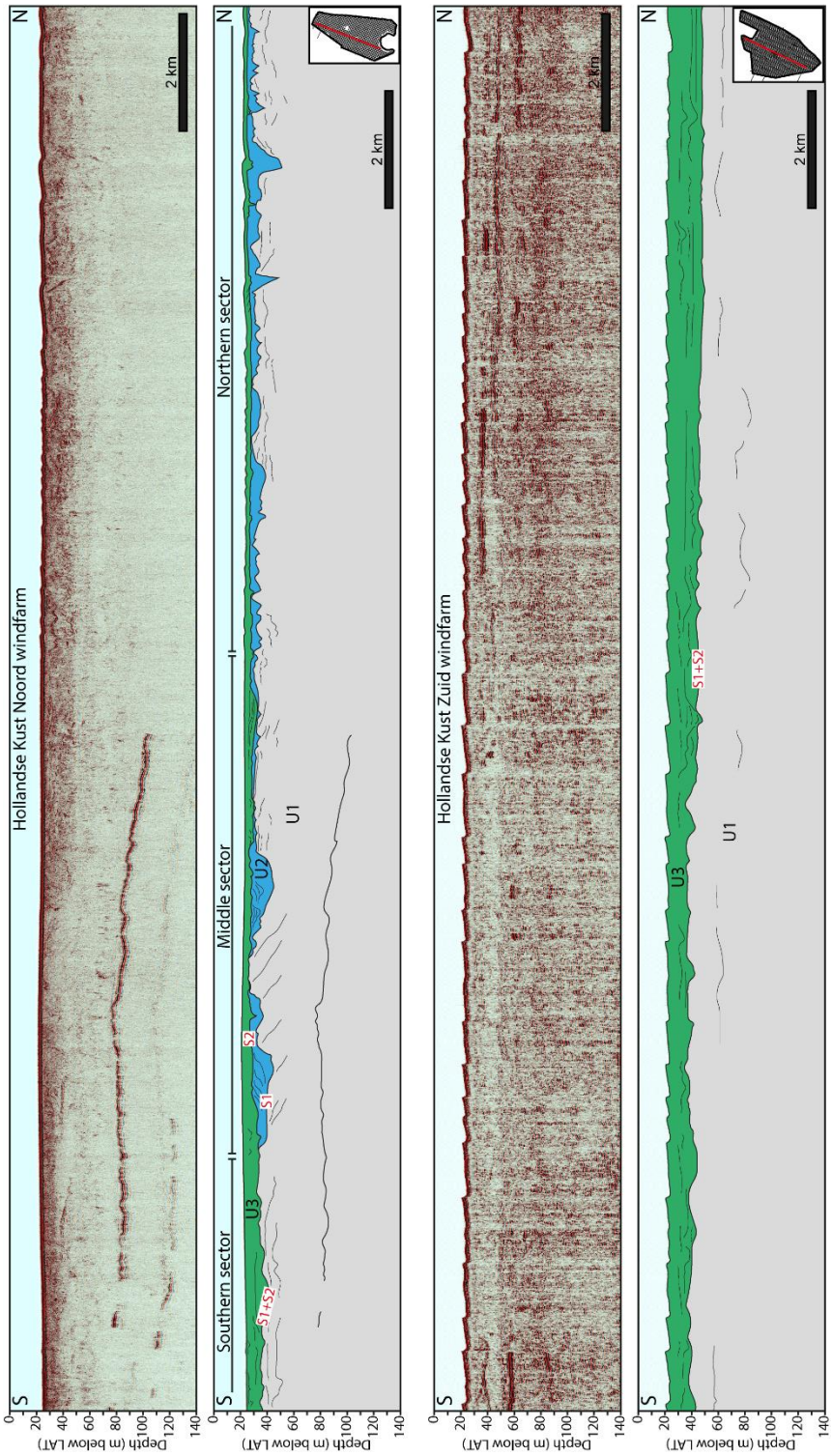
Hollandse Kust Noord windfarm
Southern sector
Middle sector
Northern sector
Hollandse Kust Zuid windfarm
S
N
U1
U2
U3
S1
S2
S1+S2
2 km
Depth (m below LAT)
0
20
40
60
80
100
120
140

Figure 3

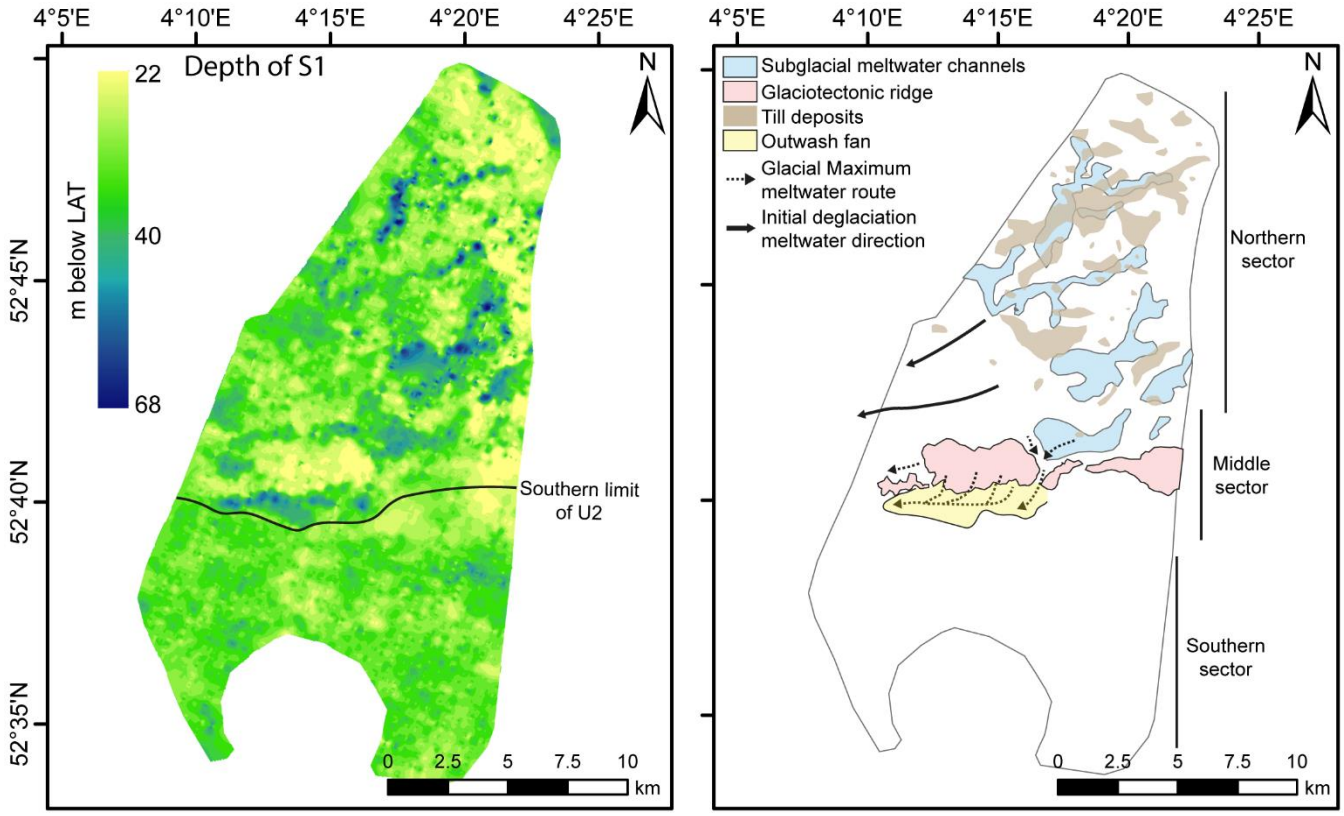
4°5'E
4°10'E
4°15'E
4°20'E
4°25'E
52°45'N
52°40'N
52°35'N
Depth of S1
22
40
68
m below LAT
N
Southern limit of U2
0
2.5
5
7.5
10
km
Subglacial meltwater channels
Glaciotectonic ridge
Till deposits
Outwash fan
Glacial Maximum meltwater route
Initial deglaciation meltwater direction
Northern sector
Middle sector
Southern sector

865

Figure 4

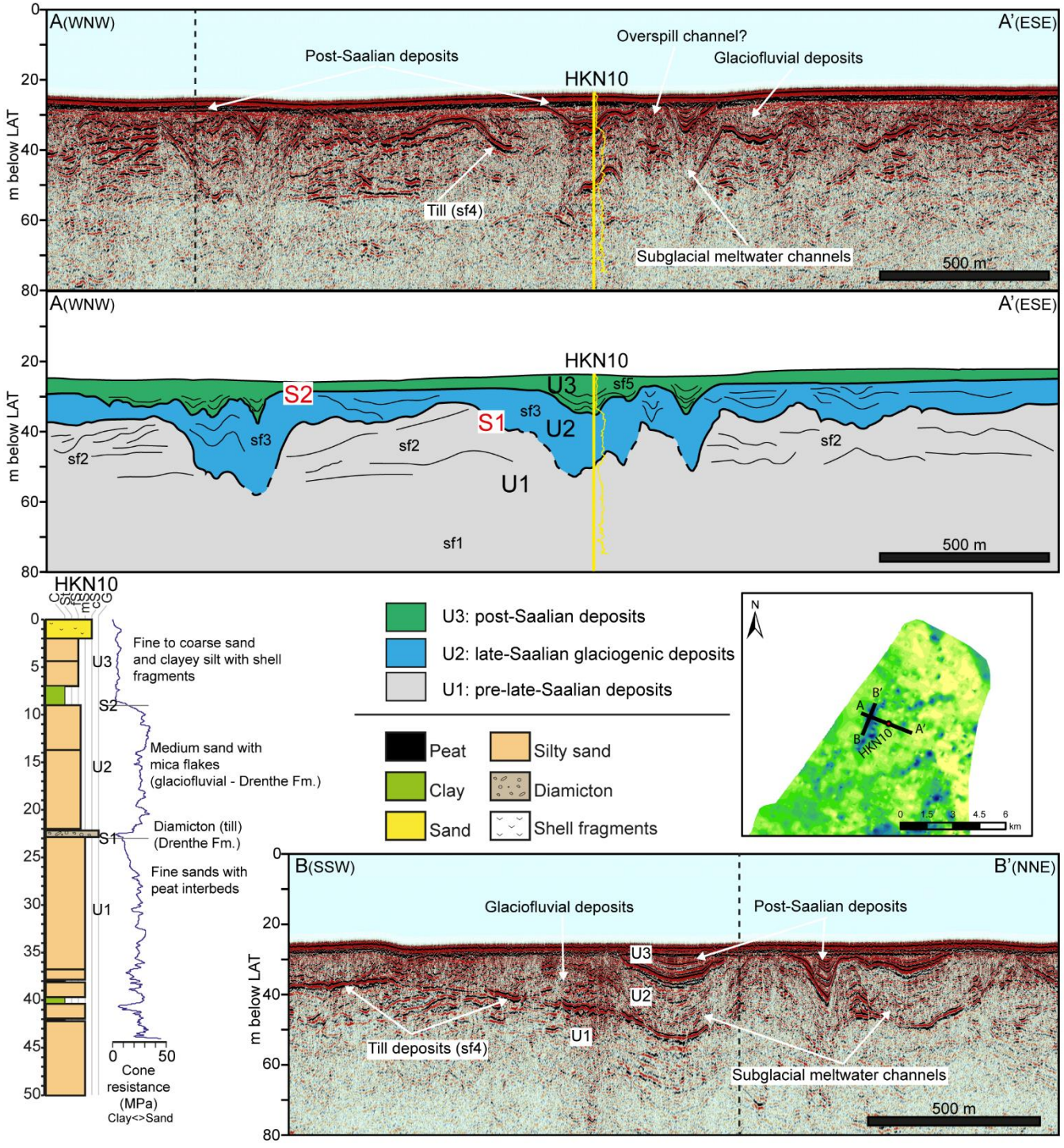
A(WNW)
A'(ESE)
Post-Saalian deposits
Overspill channel?
Glaciofluvial deposits
HKN10
Till (sf4)
Subglacial meltwater channels
500 m
m below LAT
S2
S1
U3
U2
U1
sf1
sf2
sf3
sf5
HKN10
U3: post-Saalian deposits
U2: late-Saalian glaciogenic deposits
U1: pre-late-Saalian deposits
Peat
Clay
Sand
Silty sand
Diamicton
Shell fragments
Fine to coarse sand and clayey silt with shell fragments
Medium sand with mica flakes (glaciofluvial - Drenthe Fm.)
Diamicton (till) (Drenthe Fm.)
Fine sands with peat interbeds
Cone resistance (MPa)
Clay<>Sand
N
B(SSW)
B'(NNE)
Glaciofluvial deposits
Post-Saalian deposits
Till deposits (sf4)
Subglacial meltwater channels
km

Figure 5

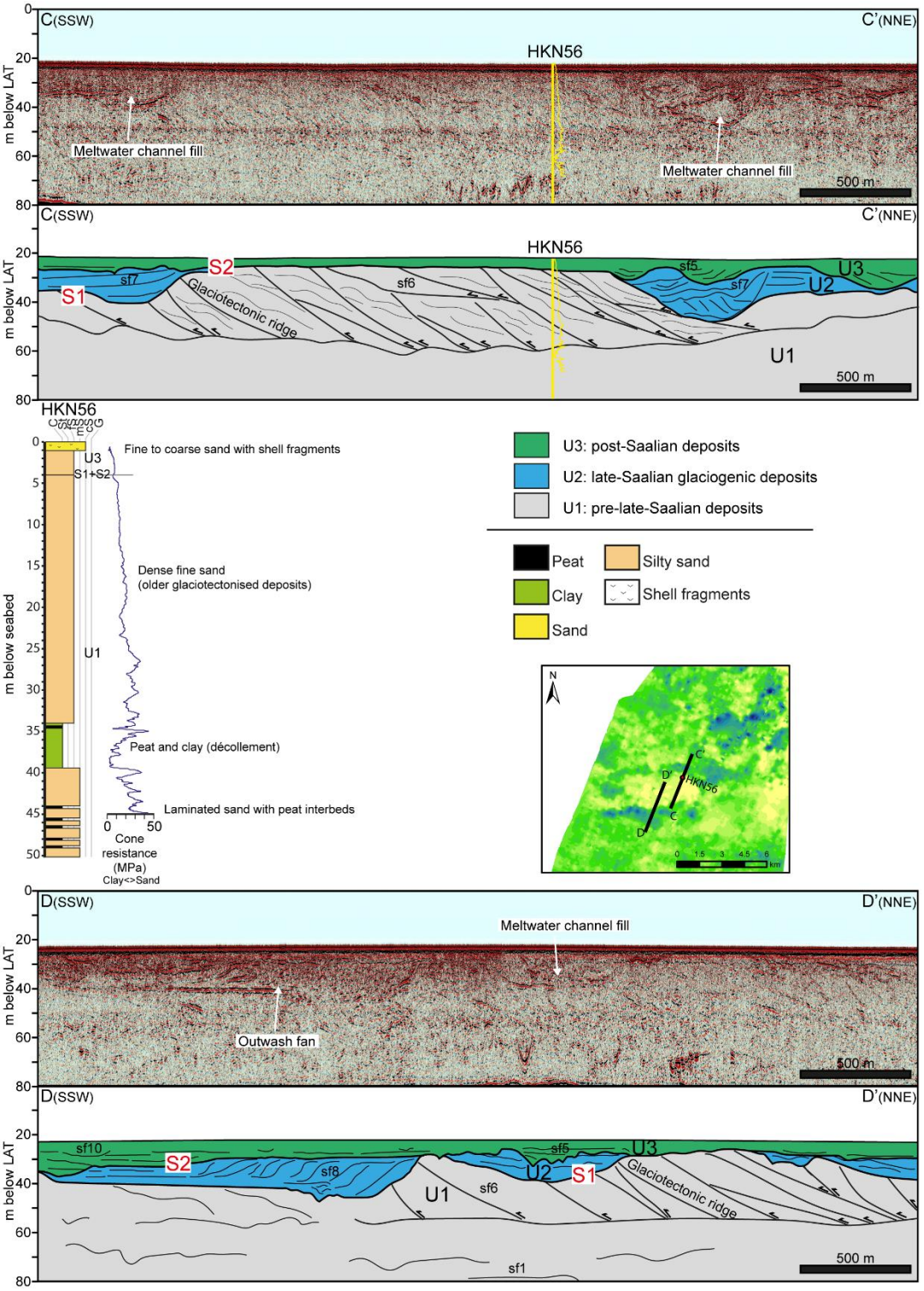
C(SSW)
C'(NNE)
HKN56
m below LAT
Meltwater channel fill
Meltwater channel fill
500 m
S1
S2
sf7
sf6
sf5
U1
U2
U3
Glaciotectonic ridge
m below seabed
Fine to coarse sand with shell fragments
Dense fine sand
(older glaciotectonised deposits)
Peat and clay (décollement)
Laminated sand with peat interbeds
Cone resistance (MPa)
Clay<>Sand
U3: post-Saalian deposits
U2: late-Saalian glaciogenic deposits
U1: pre-late-Saalian deposits
Peat
Silty sand
Clay
Shell fragments
Sand
N
D(SSW)
D'(NNE)
Outwash fan
sf10
sf8
sf1

870

Figure 6

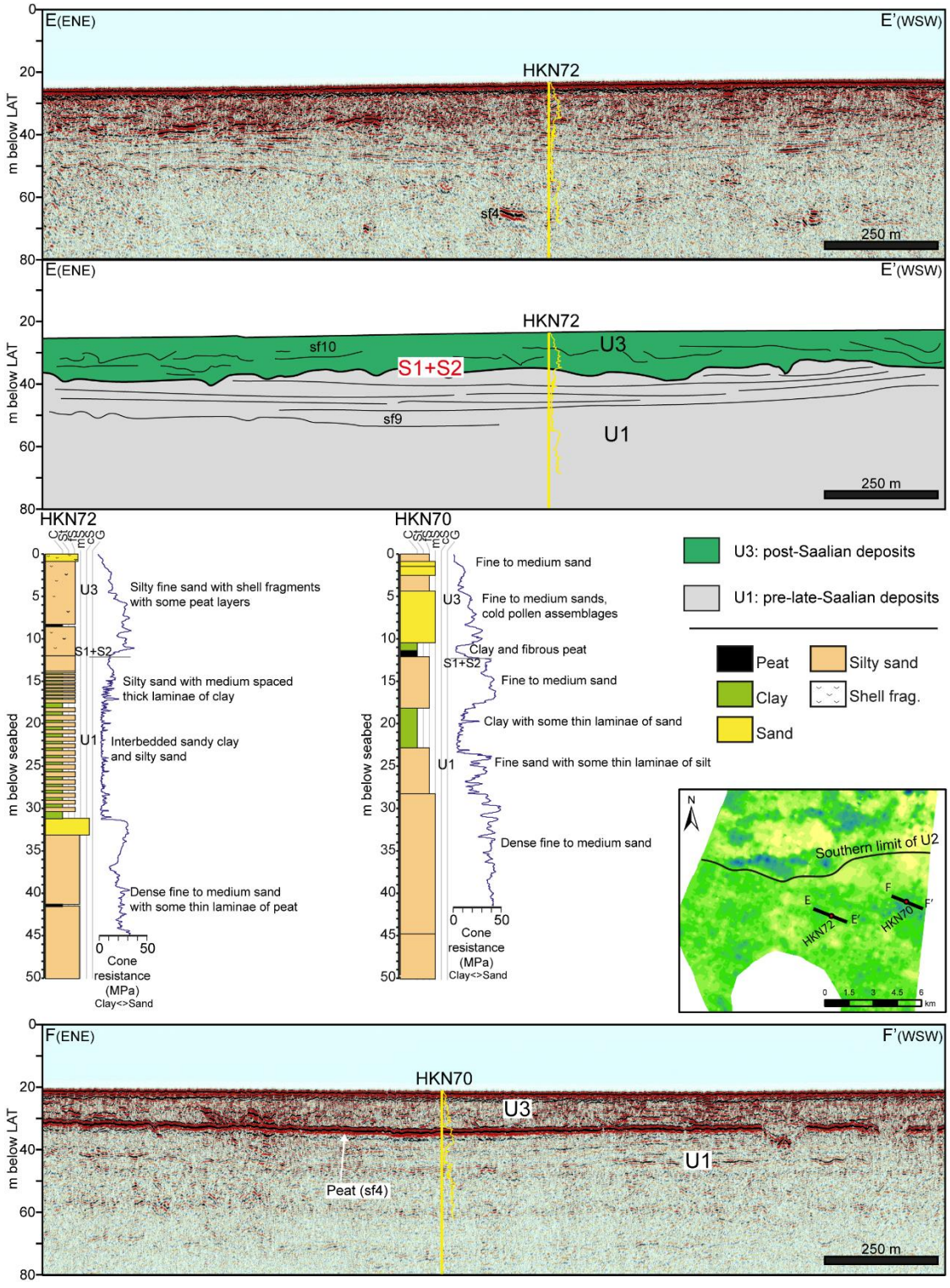
E(ENE)
E'(WSW)
HKN72
sf4
250 m
m below LAT
sf10
S1+S2
U3
sf9
U1
HKN72
HKN70
m below seabed
Silty fine sand with shell fragments with some peat layers
Silty sand with medium spaced thick laminae of clay
Interbedded sandy clay and silty sand
Dense fine to medium sand with some thin laminae of peat
Fine to medium sand
Fine to medium sands, cold pollen assemblages
Clay and fibrous peat
Fine to medium sand
Clay with some thin laminae of sand
Fine sand with some thin laminae of silt
Dense fine to medium sand
Cone resistance (MPa)
Clay<>Sand
U3: post-Saalian deposits
U1: pre-late-Saalian deposits
Peat
Silty sand
Clay
Shell frag.
Sand
N
Southern limit of U2
F(ENE)
F'(WSW)
Peat (sf4)
km

Figure 7

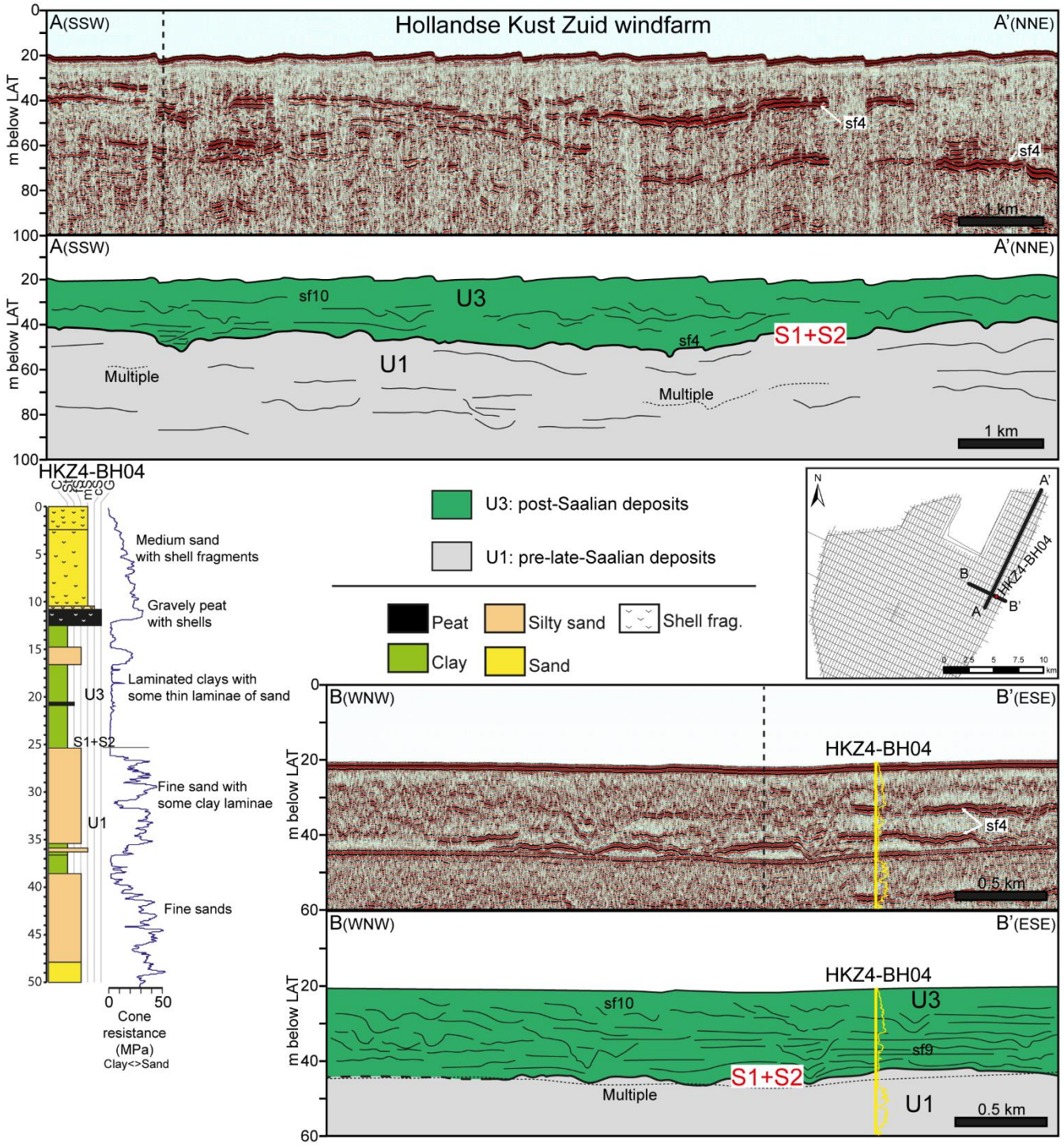
Hollandse Kust Zuid windfarm
A(SSW)
A'(NNE)
m below LAT
sf4
1 km
sf10
U3
S1+S2
U1
Multiple
HKZ4-BH04
Medium sand with shell fragments
Gravely peat with shells
Laminated clays with some thin laminae of sand
Fine sand with some clay laminae
Fine sands
Cone resistance (MPa)
Clay<>Sand
U3: post-Saalian deposits
U1: pre-late-Saalian deposits
Peat
Silty sand
Shell frag.
Clay
Sand
N
B(WNW)
B'(ESE)
0.5 km
sf9

875

Figure 8

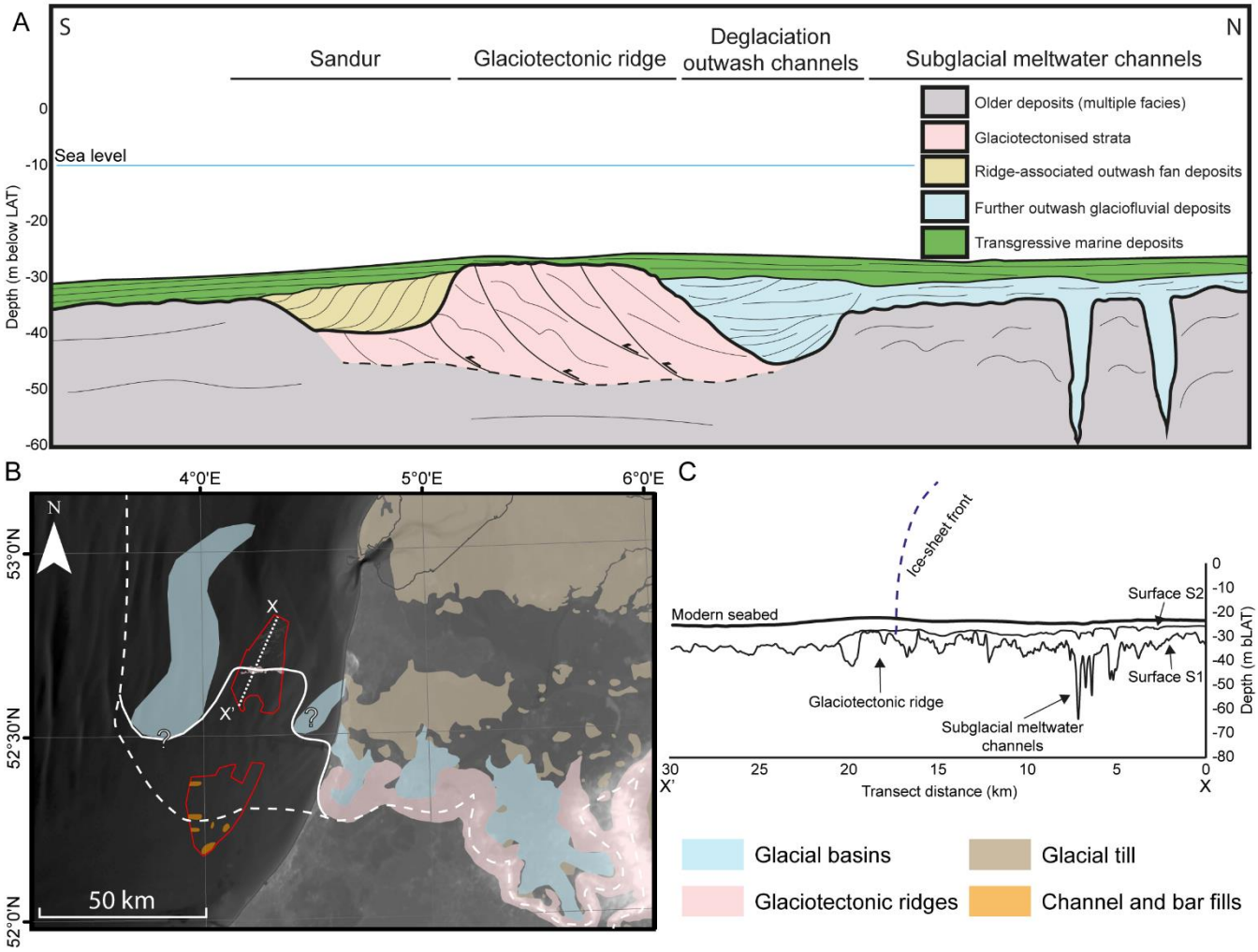
A
S
N
Sandur
Glaciotectonic ridge
Deglaciation outwash channels
Subglacial meltwater channels
Older deposits (multiple facies)
Glaciotectonised strata
Ridge-associated outwash fan deposits
Further outwash glaciofluvial deposits
Transgressive marine deposits
Sea level
Depth (m below LAT)
0
-10
-20
-30
-40
-50
-60
B
4°0'E
5°0'E
6°0'E
53°0'N
52°30'N
52°0'N
N
X
X'
50 km
C
Ice-sheet front
Modern seabed
Surface S2
Surface S1
Glaciotectonic ridge
Subglacial meltwater channels
Depth (m bLAT)
0
-10
-20
-30
-40
-50
-60
-70
-80
30
25
20
15
10
5
0
X'
X
Transect distance (km)
Glacial basins
Glacial till
Glaciotectonic ridges
Channel and bar fills

Figure 9

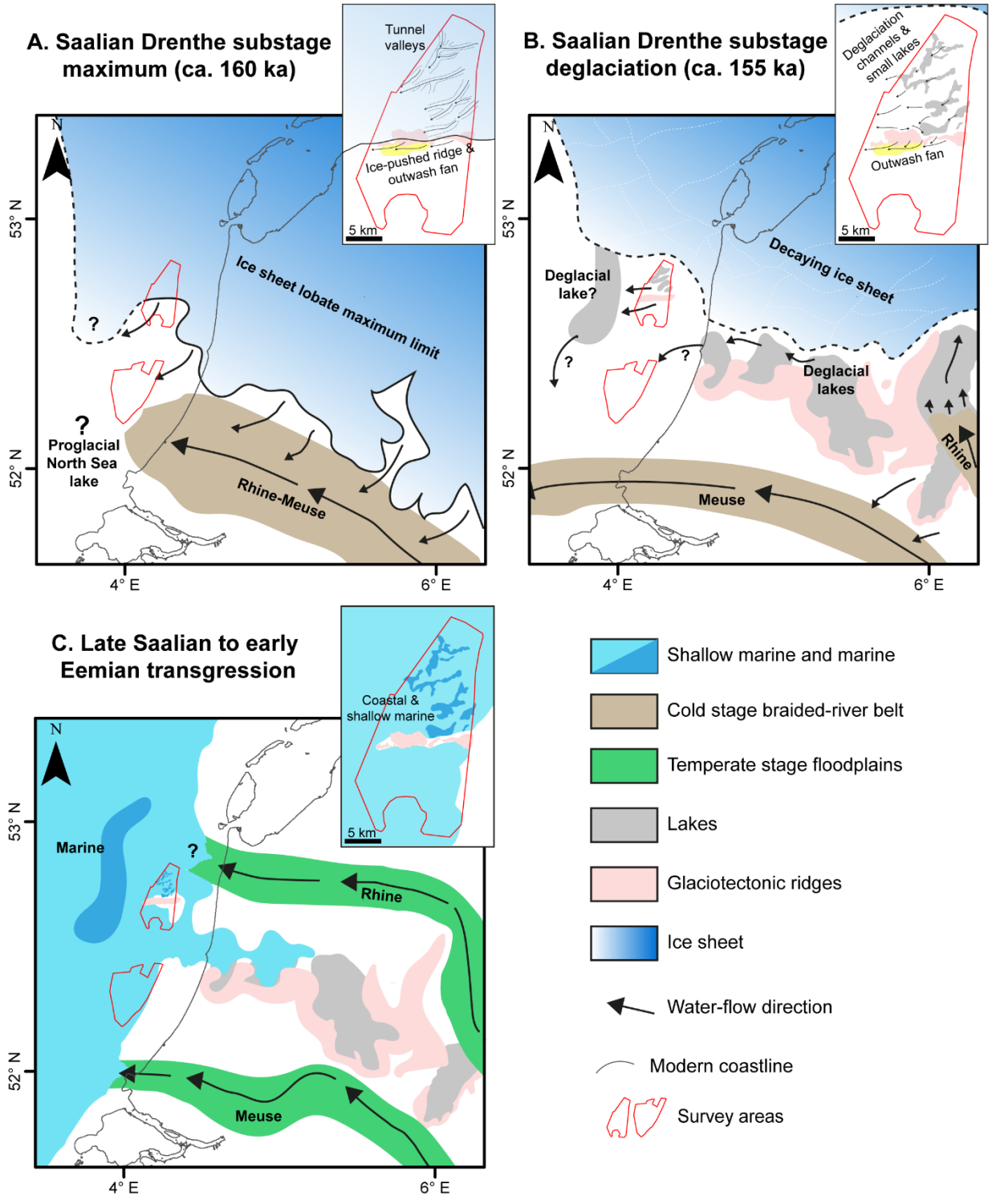
A. Saalian Drenthe substage maximum (ca. 160 ka)
Tunnel valleys
Ice-pushed ridge & outwash fan
5 km
N
53° N
52° N
4° E
6° E
Ice sheet lobate maximum limit
?
Proglacial North Sea lake
Rhine-Meuse
B. Saalian Drenthe substage deglaciation (ca. 155 ka)
Deglaciation channels & small lakes
Outwash fan
5 km
Decaying ice sheet
Deglacial lake?
Deglacial lakes
Rhine
Meuse
C. Late Saalian to early Eemian transgression
Coastal & shallow marine
5 km
Marine
Rhine
Meuse
Shallow marine and marine
Cold stage braided-river belt
Temperate stage floodplains
Lakes
Glaciotectonic ridges
Ice sheet
Water-flow direction
Modern coastline
Survey areas

880